

Effects of silica-based nanostructures with raspberry-like morphology and surfactant on the interfacial behavior of light, medium, and heavy crude oils at oil-aqueous interfaces

Lingyun Bai¹ · Chunyan Li¹ · Caroline Korte¹ · Britta M. J. Huibers¹ · Ashley R. Pales¹ · Wei-zhen Liang¹ · David Ladner¹ · Hugh Daigle² · Christophe J. G. Darnault¹

Received: 17 August 2017 / Accepted: 6 November 2017 / Published online: 18 November 2017
© The Author(s) 2017. This article is an open access publication

Abstract Any efficient exploitation of new petroleum reservoirs necessitates developing methods to mobilize the crude oils from such reservoirs. Here silicon dioxide nanoparticles (SiO₂ NPs) were used to improve the efficiency of the chemical-enhanced oil recovery process that uses surfactant flooding. Specifically, SiO₂ NPs (i.e., 0, 0.001, 0.005, 0.01, 0.05, and 0.1 wt%) and Tween[®]20, a nonionic surfactant, at 0, 0.5, and 2 critical micelle concentration (CMC) were varied to determine their effect on the stability of nanofluids and the interfacial tension (IFT) at the oil–aqueous interface for 5 wt% brine-surfactant-SiO₂ nanofluid-oil systems for West Texas Intermediate light crude oil, Prudhoe Bay medium crude oil, and Lloydminster heavy crude oil. Our study demonstrates that SiO₂ NPs may either decrease, increase the IFT of the brine-surfactant-oil systems, or exhibit no effects at all. For the brine-surfactant-oil systems, the constituents of the oil and aqueous substances affected the IFT behavior, with the nanoparticles causing a contrast in IFT trends according to the type of crude oil. For the light oil system (0.5 and 2 CMC Tween[®]20), the IFT increased as a function of SiO₂ NP concentration, while a threshold concentration of SiO₂ NPs was observed for the medium (0.5 and 2 CMC

Tween[®]20) and heavy (2 CMC Tween[®]20) oil systems in terms of IFT trends. Concentrations below the SiO₂ NP threshold concentration resulted in a decrease in IFT, and concentrations above this threshold resulted in an increase in IFT. The IFT decreased until the NP concentration reached a threshold concentration where synergetic effects between nonionic surfactants and SiO₂ NPs are the opposite and result in antagonistic effects. Adsorption of both SiO₂ NPs and surfactants at an interface caused a synergistic effect and an increased reduction in IFT. The effectiveness of the brine-surfactant-SiO₂ nanofluids in decreasing the IFT between the oil-aqueous phase for the three tested crude oils were ranked as follows: (1) Prudhoe Bay > (2) Lloydminster > and (3) West Texas Intermediate. The level of asphaltenes and resins in these crude oil samples reflected these rankings. A decrease in the IFT also indicated the potential of the SiO₂ NPs to decrease capillary pressure and induce the movement and recovery of oil in original water-wet reservoirs. Conversely, an increase in IFT indicated the potential of SiO₂ NPs to increase capillary pressure and oil recovery in reservoirs subject to wettability reversal under water-wet conditions. Raspberry-like morphology particles were discovered in 5 wt% brine-surfactant-SiO₂ nanofluid-oil systems. The development of raspberry-like particles material with high surface area, high salt stability, and high capability of interfaces alteration and therefore wettability changes offers a wide range of applications in the fields of applied nanoscience, environmental engineering, and petroleum engineering.

✉ Christophe J. G. Darnault
cdarnau@clemson.edu

¹ Department of Environmental Engineering and Earth Sciences, Laboratory of Hydrogeoscience and Biological Engineering, L.G. Rich Environmental Laboratory, Clemson University, 342 Computer Court, Anderson, SC 29625, USA

² Department of Petroleum and Geosystems Engineering, University of Texas at Austin, 200 E Dean Keeton Street, Stop C0300, Austin, TX 78712, USA

Keywords Nanomaterials · Multiphase fluids · Interfacial processes · Adsorption · Crude oils · Tween[®]20 · Enhanced oil recovery (EOR) · Raspberry-like morphology particles

Introduction

Any efficient exploitation of new petroleum reservoirs necessitates developing methods to mobilize the crude oils from such reservoirs. The traditional oil recovery process consists of a primary and a secondary phase. The primary phase is induced by natural pressure which causes oil to flow from a reservoir. As pressure decreases beyond a specific threshold, the oil will no longer flow automatically from the reservoir. In order to increase pressure in the reservoir, during the secondary phase, gas or water is injected into the reservoir (Park et al. 2015). While most crude oil reservoirs are preferably oil-wet, the sweep efficiency associated with water flooding can be limiting which leads to difficulty in recovering crude oil during the secondary phase. Reports show that only 20–40% of crude oil is recovered with the primary and secondary recovery processes (Park et al. 2015; Hu et al. 2016a), indicating that more than half of the oil remains trapped in the reservoir. Capillary forces limit the mobility of oil in the reservoir during the primary and secondary recovery processes (Wu et al. 2008). Capillary pressure, which is controlled by the wettability and interfacial tension (IFT) of the oil–water system, must be regulated to allow the flow and movement of oil through the pore network of the petroleum reservoir (Bear 1988). The displacement of oil in a reservoir is improved by increasing its mobility. Therefore, enhanced oil recovery (EOR) methods, including chemical EOR, have been created and implemented to mobilize oil and increase oil recovery from petroleum reservoirs. The wettability of petroleum reservoirs is a key factor in the oil recovery process. Altering the reservoir's wettability from oil-wet to water-wet conditions induces extreme changes in displacement mechanisms (Standnes and Austad 2000a, b; Strand et al. 2003, 2008; Somasundaran and Zhang 2006; Mohan et al. 2011; Ravari et al. 2011; Tabrizy et al. 2011; Wang et al. 2011; Park et al. 2015). The kinetics of wettability in an oil reservoir are governed by the surface activity of a surfactant, which is initially influenced by solution chemistry (Jadhunandan and Morrow 1995; Strand et al. 2008; Karimi et al. 2012). Specifically, wettability influences oil displacement in porous media, and the IFT of the oil–water system controls capillary forces, shape of oil drops, oil mobilization, and consequently oil recovery (Donaldson et al. 1989; Samanta et al. 2011; Roustaei and Bagherzadeh 2013).

In recent years, nanotechnology has offered a tremendous potential for petroleum engineering, in particular, for reservoir engineering (Amaya et al. 2002; Binks 2002; Fletcher and Davis 2010; Suleimanov et al. 2011; Wang et al. 2011; Hendraningrat et al. 2013; Kasel et al. 2013; Roustaei and Bagherzadeh 2013; Zhang et al. 2014;

Joonaki and Ghanaatian 2014; Biswal et al. 2016). Chemical agents, such as surfactants, are widely used as surface modifiers in chemical EOR to increase oil recovery. Nanoparticles are in turn coupled with surfactants as stabilizers of these diverse systems. Numerous studies have been performed to characterize the stability and mobility of nanoparticles in porous media. Specifically, the effects of the physico-chemical properties of nanoparticles and the solution chemistry of nanoparticle suspensions on their stability and mobility of nanoparticles in porous media have been investigated (Chen et al. 2004; Lecoanet and Wiesner 2004; Lecoanet et al. 2004; Espinasse et al. 2007; Wang et al. 2008a, b; Jaisi et al. 2008; Liu et al. 2009; Mattison et al. 2011; Godinez and Darnault 2011; Boucharde et al. 2012; O'Carroll et al. 2013; Hendraningrat et al. 2013; Kasel et al. 2013; Mekonen et al. 2014; Zargartalebi et al. 2015). For example, nanoparticle concentration, pH, flow velocity, pore structure, and ionic strength impact the mobility of nanoparticles in porous media (Espinasse et al. 2007; Wang et al. 2008b; Uyusur et al. 2010; O'Carroll et al. 2013; Lanphere et al. 2014; Mekonen et al. 2014). Chemicals (e.g., surfactants and polymers) have been employed to control the aggregation of nanoparticles by stabilizing them in suspension and potentially enhancing their mobility in porous media (Fu and Sun 2003; Matarredona et al. 2003; Binks and Whitby 2005; Hyung et al. 2007; Uyusur et al. 2010; Godinez and Darnault 2011; Lin et al. 2012; Fang et al. 2013; Godinez et al. 2013; Lanphere et al. 2014). Surfactants produce thermodynamically stable nanoparticles through steric repulsion among nanoparticles, thereby reducing aggregation (Jiang et al. 2003; Chen et al. 2004; Ghadimi and Metselaar 2013). Surfactants also influence the interaction between nanoparticles and surfaces, flow hydrodynamics, and rheological properties of nanofluids (Uyusur et al. 2010; Godinez and Darnault 2011; Godinez et al. 2013; Yu et al. 2014; Pales et al. 2017).

Interfacial activities play a critical role in the behavior of many complex fluids. However, very few studies have been undertaken to investigate the interfacial behavior of oil–water systems in the presence of nanoparticles and surfactants. Consequently, although there is a limited understanding of the dynamics of a system when nanoparticles are present, the coexistence of a surfactant and nanoparticles may affect the surface activities of both surfactant and nanoparticles (Ravera et al. 2006, 2008). The ability of silicon dioxide nanoparticles (SiO₂ NPs) to alter the wettability of the reservoir and reduce the IFT between crude oil and brine has recently been applied to EOR (Elder et al. 2001; Eskandar et al. 2007; Roustaei and Bagherzadeh 2013, 2015; Zargartalebi et al. 2014; Hendraningrat and Torsæter 2015a, b; Biswal and Singh 2016; Sharma et al. 2016; Huibers et al. 2017). However,

knowledge of the displacement efficiency of the SiO₂ NPs in EOR with different types of oil (light, medium, and heavy crude oils) is scarce. In their investigation of the influence of SiO₂ NPs on the properties of the anionic surfactant sodium dodecyl sulfate (SDS), Zargartalebi et al. (2014) observed that the addition of SiO₂ NPs affected the interfacial and adsorption properties of the surfactant. Opposite interfacial behaviors for oil and nano-augmented surfactant systems were also observed with low and high concentrations of the anionic surfactant. Ma et al. (2008) studied the effects of SiO₂ NPs and non-ionic (Triton X-100) and SDS surfactants on trichloroethylene (TCE)-water interfaces. The addition of SiO₂ NPs slightly increased the efficiency of SDS at low concentrations and reduced IFT at TCE-water interfaces. However, SiO₂ NPs did not influence the IFT at TCE-water interfaces in the presence of Triton X-100. Electrostatic repulsion between negatively charged SiO₂ NPs and SDS was established as the controlling factor of this IFT behavior. Ravera et al. (2006, 2008) reported on the effects of SiO₂ NPs on the interfacial behavior between a cationic surfactant (CTAB, hexadecyltrimethylammonium bromide) and hexane. An increase in SiO₂ NPs concentration in CTAB induced an increase in IFT between SiO₂ NPs–CTAB and hexane. This phenomenon was attributed to the adsorption of CTAB on SiO₂ NPs and the resulting restructuring of the nanoparticle-surfactant layer.

Research on the effects of ZrO₂ NPs on the interfacial behavior of surfactant solutions (i.e., SDS, lauryl alcohol 7 mol ethoxylate (nonionic), and dodecyl trimethyl ammonium bromide (cationic)) and n-heptane-water interfaces demonstrated that below the critical micelle concentration (CMC) of the studied surfactants, increases in nanoparticle concentrations impacted the surface activity of the surfactant and induced a decrease in IFT (Esmaeilzadeh et al. 2014). However, no impact of ZrO₂ NPs on the IFT between the surfactant and n-heptane was detected at or above the CMC of these surfactants. Lan et al. (2007) reported the synergistic effect of SiO₂ NPs and CTAB on the stability of oil–water emulsions. The established reduction effect of SiO₂ NPs on the IFT of oil–water in the presence of CTAB may be caused by the increase in surfactant adsorption due to electrostatic interactions between adsorbed particles and bulk surfactant molecules. Results also show that SiO₂ NPs were adsorbed at the oil–water interface with an appropriate amount of CTAB, but were desorbed into the bulk solution as flocs with excessive CTAB concentration. Interactions of SiO₂ NPs and surfactants (lecithin or oleylamine) at oil–water interfaces were studied for different polarities of oil phases (Miglyol®812 or liquid paraffin) (Eskandar et al. 2007). The concentration of SiO₂ NPs governed the increase or decrease in the IFT of oil–water systems as a result of

either attracting the surfactant to the oil–water interface or depleting the surfactant from the oil–water interface. As nanoparticles can self-assemble at the interface between oil and water systems, knowledge of the assembly and interactions between nanoparticles and surfactants is fundamental. Therefore, understanding the synergetic or antagonistic effects of nanoparticles on a surfactant is critical. However, sufficient information is unavailable about the properties of these nanoparticle-surfactant systems, such as their stability and interfacial behavior in association with various types of crude oil.

Understanding the mechanisms that govern the dynamics at these interfaces is a critical component of the management and exploitation of oil reservoirs. This understanding is essential for modifying the properties of nanofluids for specific fluid science and engineering applications, particularly the use of nanofluids in nanoparticle engineering for subsurface processes such as EOR. All of the possible factors (e.g., aggregation, surface charge, sedimentation of nanoparticles) have yet to be seriously considered in any study. Consequently, critical gaps remain in our knowledge of the IFT alterations of oil-aqueous systems caused by nanoparticle dispersion in crude oil. Among the many nanoparticles that are utilized in EOR, metal oxide nanoparticles, such as SiO₂ NPs, are of particular interest because SiO₂ based nanofluids have been shown to significantly increase oil recovery yield during an EOR process (Hendraningrat and Torsæter 2014, 2015b; Griffith et al. 2016). In this context, the primary objectives of this research are to (1) explore the ability of SiO₂ NPs to improve the efficiency of the chemical EOR that uses surfactant flooding, (2) investigate how varying SiO₂ NPs and surfactant concentrations impact the stability of nanofluids and alter the IFT between nanofluids and crude oils for EOR—light crude oil, West Texas Intermediate; medium crude oil, Prudhoe Bay; and heavy crude oil, Lloydminster, and (3) establish the properties of crude oils that influence the dynamic and equilibrium behaviors of IFT at the oil-aqueous interface for brine-surfactant-SiO₂ nanofluid-oil systems.

Materials and methods

Nanoparticles

Fumed silicon dioxide (SiO₂) nanopowder, supplied by PlasmaChem GmbH (Berlin, Germany) was used as the hydrophilic nanoparticle material. The material consists of more than 99.8% SiO₂ with an average nanoparticle size of 7–14 nm, a bulk density of 0.048 g/cm³, and a specific surface area over 200 m²/g.

Surfactant

The nonionic surfactant Tween[®]20 was obtained from Sigma-Aldrich (USA). The critical micelle concentration (CMC) of Tween[®]20 is 60 mg/L with a density of 1.095 g/mL at 25 °C and a molecular weight of 1228 g/mol. The hydrophile-lipophile balance (HLB) value for Tween[®]20 is 16.7.

Crude oils

Three types of crude oil (light oil, West Texas Intermediate (Environment Canada 2017a); medium oil, Prudhoe Bay (Environment Canada 2017b); and heavy oil, Lloydminster (Environment Canada 2017c) were used to simulate the oil phase. The physical and chemical properties of the crude oils are listed in Table 1.

Nanofluid preparation

Three stock solutions were prepared for the dispersion of nanofluids: a base aqueous fluid, consisting only of 5% brine (Tween[®]20 concentration of 0 CMC), and two brine-surfactant solutions with Tween[®]20 concentrations of 0.5 CMC and 2 CMC. The synthetic reservoir brine was the major component of the base aqueous fluid for nanoparticle dispersion. The 5 wt% brine base solution was prepared by adding 52.6316 g of NaCl (Fisher Scientific, Waltham, MA) into 1000 mL of ultrapure deionized (DI) water (resistivity > 18.2 MΩ cm, Millipore Corporation, Billerica, MA). The specified amounts of NaCl were weighted using a NewClassic MF analytical balance (Mettler Toledo, Columbus, OH). The brine solution was completely mixed using a laboratory stirrer (Model PC-310, Corning Inc., Corning, NY) for 10 min. The two brine-surfactant solutions were prepared by injecting two concentrations of Tween[®]20, 0.5 CMC and 2 CMC, into 5 wt% brine solution. To make the 5 wt% brine with 0.5 CMC Tween[®]20, 27.4 μL Tween[®]20 was added to 1000 mL 5 wt% brine.

To generate the 5 wt% brine with 0.5 CMC Tween[®]20, 109.6 μL Tween[®]20 was added to 1000 mL 5 wt% brine.

A series of SiO₂ NPs concentrations were then dispersed in the three aqueous phases (0, 0.5, and 2 CMC brine-surfactant solutions). Five 100 mL solutions of each brine-surfactant solution were transferred into 100 mL beakers. Stock suspensions of SiO₂ NPs at concentrations of 0.001, 0.005, 0.01, 0.05, and 0.1 wt% were then prepared according to the following dispersion protocol. Specific amounts of SiO₂ NPs (1, 5, 10.001, 50.025, and 100 mg) were weighed using an UMT2 ultra-microbalance (Mettler Toledo, Columbus, OH) in the Nano Enclosure Xpert[®], 38872 series (Labconco, Kansas City, MO) and then mixed with brine-surfactant solutions in the 100 mL beakers. Nanoparticle stock solutions with 0.001, 0.005, 0.01, 0.05, and 0.1 wt% concentrations, respectively, were produced, yielding a total of 18 different brine-surfactant-nanoparticle solutions (Table 2). Each of the nanofluid suspensions were sonicated by an ultrasonic liquid processor (Missonix, S-4000, Newton, CT), with an amplitude of 45 and a power strength of 40 W for 4 min before measuring the properties of the nanofluids (size, zeta potential, and sedimentation characteristics) and the IFT between the crude oil and the nanofluid.

Characteristics of nanofluid systems

Size of SiO₂ nanoparticles

The z-average hydrodynamic diameter and size distribution of the SiO₂ NP aggregates in each nanofluid was determined by dynamic light scattering (DLS) using a 90Plus Zeta Particle Size Analyzer (Brookhaven Instruments Corporation, Holtsville, NY). Approximately 4 mL of the sonicated SiO₂ NP suspension was transferred to a small, transparent, four-sided cuvette made of polystyrene (light path 10 mm, volume of 4.5 mL) and inserted into a small slot in a 90Plus Zeta Particle Size Analyzer. Each solution was measured for 30 min continuously at 10 s intervals.

Table 1 Physico-chemical properties and hydrocarbon mass fractions of West Texas Intermediate (Environment Canada 2017a), Prudhoe Bay (Environment Canada 2017b), and Lloydminster (Environment Canada 2017c) crude oils

Crude oil	Oil type	Density (g/ml) at 15 °C	Dynamic viscosity (mPa·s) at 15 °C	API gravity (°)	Sulphur (wt%)	Saturates (wt%)	Aromatics (wt%)	Resins (wt%)	Asphaltenes (wt%)
West Texas Intermediate	Light	0.8212 ^a	7 ^a	40.8	0.34 ^a	66 ^a	26 ^a	6 ^a	1 ^a
Prudhoe Bay	Medium	0.8837 ^b	22 ^b	28.5	0.96 ^b	53 ^b	34 ^b	10 ^b	4 ^b
Lloydminster	Heavy	0.9020 ^a	63	20.7	3.15	68 ^a	22 ^a	4 ^a	6 ^a

^aAt evaporation (volume %: 0)

^bAt evaporation (weight %: 0)

Table 2 The 18 nanofluid systems created for experimentation including three types of oil with six concentrations of nanoparticles either with or without surfactant

Oil type	Surfactant and nanoparticle concentration		
	5% Brine	5% Brine + 0.5 CMC Tween [®] 20	5% Brine + 2 CMC Tween [®] 20
West Texas Intermediate	0 wt% NP	0 wt% NP	0 wt% NP
	0.001 wt% NP	0.001 wt% NP	0.001 wt% NP
	0.005 wt% NP	0.005 wt% NP	0.005 wt% NP
	0.01 wt% NP	0.01 wt% NP	0.01 wt% NP
	0.05 wt% NP	0.05 wt% NP	0.05 wt% NP
	0.1 wt% NP	0.1 wt% NP	0.1 wt% NP
Prudhoe Bay	0 wt% NP	0 wt% NP	0 wt% NP
	0.001 wt% NP	0.001 wt% NP	0.001 wt% NP
	0.005 wt% NP	0.005 wt% NP	0.005 wt% NP
	0.01 wt% NP	0.01 wt% NP	0.01 wt% NP
	0.05 wt% NP	0.05 wt% NP	0.05 wt% NP
	0.1 wt% NP	0.1 wt% NP	0.1 wt% NP
Lloydminster	0 wt% NP	0 wt% NP	0 wt% NP
	0.001 wt% NP	0.001 wt% NP	0.001 wt% NP
	0.005 wt% NP	0.005 wt% NP	0.005 wt% NP
	0.01 wt% NP	0.01 wt% NP	0.01 wt% NP
	0.05 wt% NP	0.05 wt% NP	0.05 wt% NP
	0.1 wt% NP	0.1 wt% NP	0.1 wt% NP

The size measurement data were collected using the corresponding software, BIC Particle Sizing Software.

Morphology of SiO₂ nanoparticles

Scanning electron microscope (SEM) was used to characterize the morphology of SiO₂ nanoparticles. Scanning electron microscope (SEM) images of SiO₂ nanoparticles of representative nanofluid systems were obtained using a Hitachi S-4800 SEM. SEM images of SiO₂ nanoparticles were acquired under 4 kV and 500 nm resolutions for the following nanofluid systems: (a) brine-0.001% SiO₂ NPs; (b) brine-0.5 CMC Tween[®]20-0.001% SiO₂ NPs; (c) brine-2 CMC Tween[®]20-0.001% SiO₂ NPs; (d) brine-0.01% SiO₂ NPs; (e) brine-0.5 CMC Tween[®]20-0.01% SiO₂ NPs; (f) brine-2 CMC Tween[®]20-0.01% SiO₂ NPs; (g) brine-0.1% SiO₂ NPs; (h) brine-0.5 CMC Tween[®]20-0.1% SiO₂ NPs; and (i) brine-2 CMC Tween[®]20-0.1% SiO₂ NPs.

Zeta potential of SiO₂ nanoparticles

To measure the zeta potential of the SiO₂ NP aggregates for each nanofluid, 2 mL of the sonicated solution was transferred into a polystyrene cuvette and placed into a small slot in a 90Plus Zeta Particle Size Analyzer. Each solution was measured for 30 min continuously at 5 min

intervals. The data for the zeta potential measurement were collected using a BIC PALS Zeta Potential Analyzer.

Sedimentation of SiO₂ nanoparticles

Sedimentation characteristics of the SiO₂ NPs suspensions were obtained from UV–Vis spectroscopy measurements using a Cary 300 Bio UV–Visible Spectrophotometer (formerly Varian, Walnut Creek, CA; now Agilent, Santa Clara, CA). UV–Vis measurements were conducted by placing the SiO₂ NPs suspensions within a Spectrosil[®] spectrophotometer cell (VWR, Radnor, PA) with a dimension of 12.5 W × 12.5L × 25H mm, volume of 0.7 mL, and made of Spectrosil[®] quartz, which has a wavelength range of 170–2700 nm at 25 °C. Solutions without SiO₂ NPs were used as blank solutions, and standard UV–Vis SiO₂ NP absorbance data were monitored to determine the sedimentation rate of the SiO₂ NPs under the influence of brine and Tween[®]20. UV–Vis measurements were carried out after sonication of the nanofluids. Data were collected every 10 s continuously for 30 min. The evaluation of the stability of nanofluids was also conducted using direct visual observations of the nanoparticles in the brine-surfactant systems at different time intervals after sonication of each set of nanofluids (0, 20, and 30 min).

Surface tension measurements of brine-surfactant-SiO₂ nanofluid systems and crude oils

Surface tension measurements were carried out with the DSA25 Drop Shape Analyzer (Kruss GmbH, Germany) in pendant drop mode with dynamic changes in surface tension tracked as a function of time for 30 min at 10-s intervals. The sonicated nanofluids were placed in a plastic syringe (1 mL NORM-JECT Tuberkulin syringe, Fisher Scientific, Waltman, MA) with a steel needle. A drop of nanofluid was suspended from the tip of the steel needle, and Data Shape Analysis software was used to track surface tension data between the air and the nanofluid every 10 s for 30 min. During the measurement, the contour of the nanofluid drop image was extracted to calculate surface tension values by the Young–Laplace equation. The mean value of triplicate measurements was reported as a final surface tension value. The same procedure was used to measure the surface tension of the three oil types.

Interfacial tension measurements of brine-surfactant-SiO₂ nanofluid-oil systems

The IFT between the crude oil drops and brine, brine-surfactant solutions, and SiO₂ nanofluids was measured using the DSA25 Drop Shape Analyzer (Kruss GmbH, Germany) at 20 °C (Fig. 1a). 20 mL of sonicated solution was placed in a glass cuvette made with optical glass with an inner dimension of 36 W × 36D × 30 H mm. Measurements were taken on oil droplets that were hanging from the tip of a syringe (1 mL NORM-JECT Tuberkulin, Fisher Scientific, Waltman, MA) needle (J hook needle, 69 μm diameter) (Fig. 1b). The Data Shape Analysis software was used to track IFT data as a function of time, every 10 s for 30 min. During the measurement, the contour of the oil drop image was extracted to calculate IFT values by the Young–Laplace equation. Each IFT measurement was repeated three times for each brine, brine-surfactant solution, and SiO₂ nanofluid using the three oil types.

Statistical methods

The outliers of the IFT values were removed from the triplicate data based on Eqs. (1) and (2) for each 30 min IFT data series:

$$\text{Lower outlier} = Q_1 - 1.5IQ, \quad (1)$$

$$\text{Upper outlier} = Q_3 + 1.5IQ, \quad (2)$$

where Q_1 = 25th percentile, Q_3 = 75th percentile, and $IQ = Q_3 - Q_1$ (interquartile range). After preprocessing, triplicate data were averaged to represent unique IFT data for each nanofluid system.

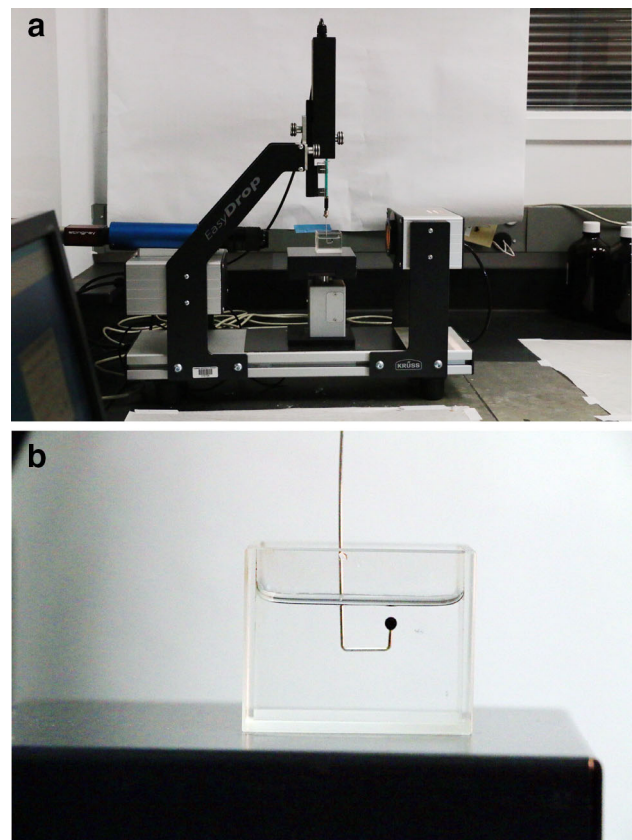


Fig. 1 Experimental equipment for interfacial tension (IFT) measurement (a) and visualization of drop of crude oil in SiO₂ nanofluid for IFT measurement (b)

The Loess model was applied to oscillating IFT data to obtain a smooth curve with a span of 0.75 using R (Version 0.99.903-© 2009–2016 RStudio, Inc.). To establish the IFT at equilibrium, the pivot time was determined for each system from the minimum of first derivatives calculated from the smoothed data. After the pivot time, the average and standard deviation of the equilibrium IFT were calculated. After removal of the outliers, all of the treatments were plotted in a smooth curve with a span of 0.75 with raw data for comparison.

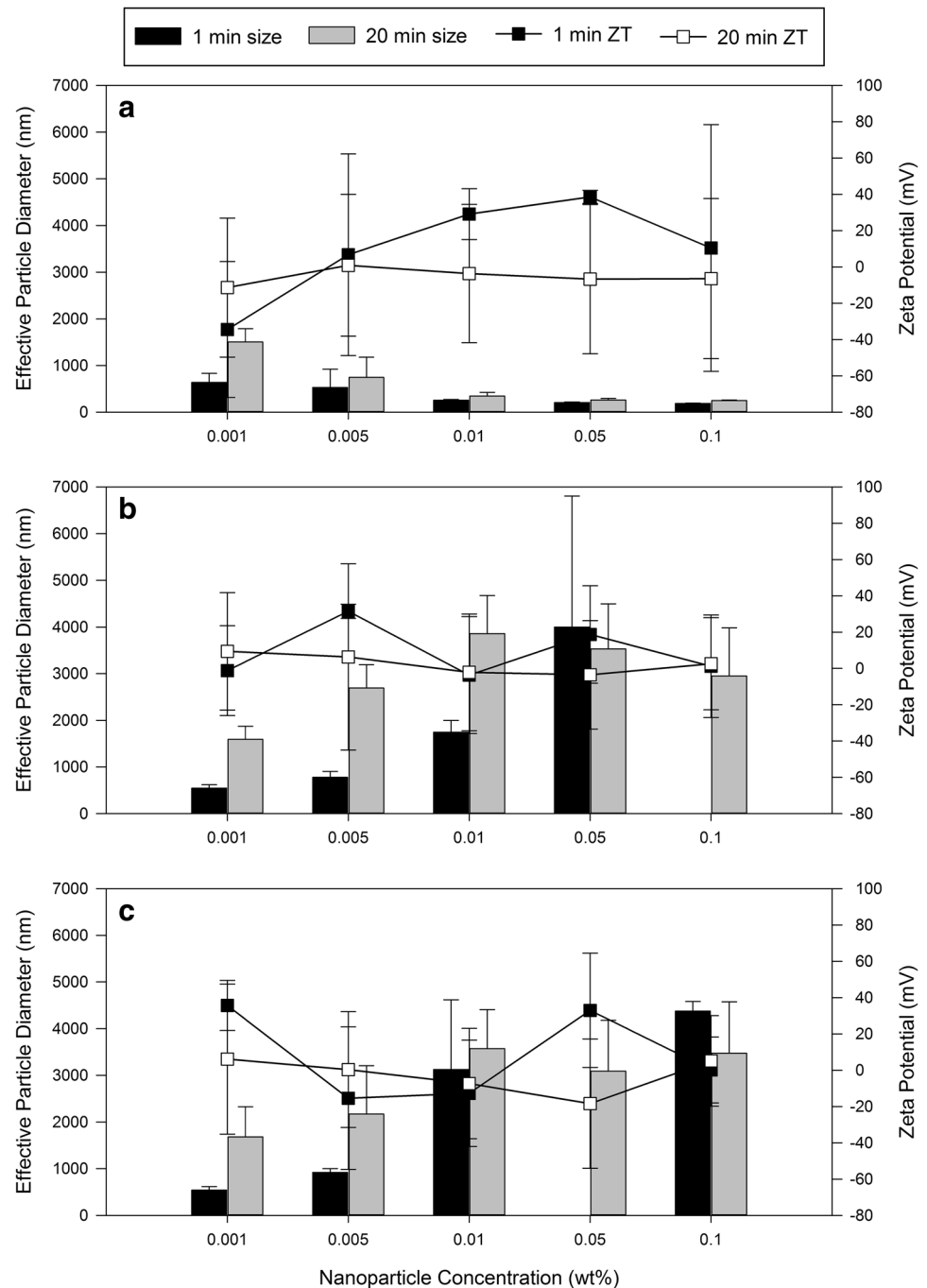
Results

Characteristics of nanofluid systems

Size and zeta potential of SiO₂ nanoparticles

The initial and equilibrium mean nanoaggregate size and the zeta potential of nanoparticle suspensions both with and without surfactant are shown in Fig. 2. The initial values were calculated by averaging the size and the zeta potential data from the first 1-min of 30 min, and the equilibrium

Fig. 2 Initial (I.) (open symbols) and equilibrium (E.) (solid symbols) behaviors of SiO₂ nanoaggregate particle size (column) and zeta potential (scatter) for brine-SiO₂ nanofluid samples with five SiO₂ nanoparticle concentrations (0.001 wt% NP, 0.005 wt% NP, 0.01 wt% NP, 0.05 wt% NP, and 0.1 wt% NP) **a** without Tween[®]20 (0 CMC), **b** stabilized with 0.5 CMC Tween[®]20, and **c** stabilized with 2 CMC Tween[®]20



values were calculated by averaging the values collected between 20 and 30 min.

The effective nanoaggregate diameter and zeta potential for nanofluids with 0.001 to 0.1 wt% SiO₂ NPs concentrations are shown in Fig. 2a. In the absence of surfactant, the size of the nanoaggregates decreased as a function of SiO₂ NPs concentration until 0.1 wt% for both the initial and equilibrium stages. The effective particle diameter decreased from 639 ± 193 to 190 ± 5 nm in the initial phase and was reduced from 1503 ± 289 to 249 ± 12 nm

in the equilibrium phase as nanoparticle concentration increased. The initial zeta potential value was -34 ± 37 mV for the 0.001 wt% nanofluid. Upon increasing the nanoparticle concentration, the nanofluid with 0.005 wt% SiO₂ NPs obtained a zeta potential of 7 ± 56 mV, 29 ± 14 mV at 0.01 wt%, and 39 ± 4 mV at 0.05 wt%. With a further increase in the concentration of nanoparticles to 0.1 wt%, the zeta potential decreased to 10 ± 68 mV. In the first 20 min, the zeta potential changed dramatically as nanoparticle concentration increased,

at which point the zeta potential values stabilized after 20 min, at approximately -10 ± 40 mV for the 0.001, 0.01, 0.05 and 0.1 wt% SiO₂ NPs, and approximately 1 ± 39 mV for the 0.005 wt% SiO₂ NPs.

The initial and equilibrium size and zeta potential of the nanofluids stabilized by 0.5 CMC and 2 CMC Tween[®]20 are shown in Fig. 2b, c. In the presence of 0.5 CMC Tween[®]20, the nanoaggregate size shows a steadily increasing trend at the initial stages from 546 ± 70 nm at 0.001 wt% SiO₂ NPs concentration to 3999 ± 2807 nm at 0.05 wt%. The size at 0.1 wt% was extremely high, beyond the measurement capability of the Zeta Particle Size Analyzer, and, thus, is not reported here. The nanofluids with 0.001 wt% to 0.01 wt% SiO₂ NPs concentration had larger particle sizes at the equilibrium stage than at the initial stage, increasing from 1593 ± 282 nm to 3860 ± 814 nm. However, as nanoparticle concentration increased to 0.1 wt%, SiO₂ NPs, the nanoaggregate sizes were smaller at the equilibrium stage than at the initial stage, ranging from 3529 ± 968 to 2951 ± 1034 nm. During the initial phase, in a 0.5 CMC Tween[®]20 nanofluid, zeta potential values tended to be unstable with increasing nanoparticle concentrations. The values were -1 ± 25 , 32 ± 4 , -4 ± 32 , 19 ± 27 and 1 ± 28 mV for the 0.001 wt% brine-surfactant-SiO₂ nanofluid through 0.01 wt%, respectively. After 20 min, all concentrations of nanofluids had a consistent zeta potential of approximately 1 ± 30 mV.

The nanoaggregate size trend of the brine-surfactant-SiO₂ nanofluid is similar for the 0.5 CMC and the 2 CMC Tween[®]20 concentrations. At 2 CMC Tween[®]20, the initial nanoaggregate size increased from 543 ± 71 nm to 3126 ± 1492 nm for the 0.001 wt% and the 0.01 wt%, respectively, and then decreased from a size over 6000 nm at 0.05 wt% to 4375 ± 207 nm at 0.1 wt%. At the equilibrium stage, the 0.001 wt% through the 0.01 wt% had larger nanoaggregate sizes than at the initial stage, ranging from 3572 ± 835 nm to 1680 ± 648 nm, respectively. At 0.05 wt%, the nanoaggregate size decreased to 3088 ± 1087 nm at the equilibrium stage. At a nanoparticle concentration of 0.1 wt%, the nanoaggregate size at the equilibrium stage was 3473 ± 1099 nm. The zeta potential of 2 CMC Tween[®]20 brine-surfactant-SiO₂ nanofluid with nanoparticle concentration between 0.001 and 0.1 wt% was unstable with values of 39 ± 14 , -15 ± 39 , -12 ± 29 , 33 ± 31 and 0 ± 18 mV, respectively. Zeta potentials for these solutions became stable after 20 min with a value of approximately 3 ± 32 mV.

The histograms of the size distribution of SiO₂ nanoparticles of the different nanofluid systems are shown in Fig. 3. In brine-SiO₂ NP systems, the lowest concentrations of nanoparticles (0.001 and 0.005 wt%) generated

a polydisperse size distribution while higher concentrations produced a monodisperse size distribution of SiO₂ NPs, in the case of the size distributions built from DLS measurements for 1 min and 20–30 min. In the brine-0.5 CMC Tween[®]20-SiO₂ NP and the brine-2 CMC Tween[®]20-SiO₂ NP systems, similar findings were observed, except that the range of SiO₂ NP concentrations for which a polydisperse size distribution was observed encompassed 0.001, 0.005 and 0.01 wt% SiO₂ NPs.

Morphology of SiO₂ nanoparticles

SEM images of SiO₂ nanoparticles are presented in Fig. 4. It can be seen that SiO₂ nanoparticles at 0.001, 0.01, and 0.1 wt% formed aggregates in the brine-SiO₂ nanofluid systems and the brine-surfactant-SiO₂ nanofluid systems. SEM images show an assemblage of SiO₂ nanoparticles where large particles are covered by small ones (Fig. 4). SEM confirms the raspberry-like morphology particles of these assemblages of SiO₂ nanoparticles.

Sedimentation of SiO₂ nanoparticles

The sedimentation study of the brine-surfactant-SiO₂ nanofluids monitored by UV–Vis spectrophotometer is based on an initial wavelength reading of 204 nm. The sedimentation results at the initial and equilibrium stages of the nanoaggregates in 15 nanofluids with SiO₂ NPs concentrations from 0.001 to 0.1 wt% are shown in Fig. 5 in the absence and presence of 0.5 CMC and 2 CMC Tween[®]20. In the absence of Tween[®]20 in all nanofluids, the initial sedimentation ratio was approximately 0.1, however, after adding Tween[®]20, the sedimentation ratio increased. The initial sedimentation ratio for the first minute after monitoring, which is calculated as an average of the measurements, was approximately 0.1 for all solutions. Although very little sedimentation occurred in the first minute, high sedimentation rates were recorded between 20 and 30 min after monitoring began. The sedimentation ratio was 0.5 at 0.001 wt%, 0.8 at 0.005 wt%, 0.7 at 0.01 wt% and 0.05 wt%, and back to 0.5 at 0.1 wt%.

The sedimentation ratios for nanofluids with 0.001 to 0.01 wt% with 0.5 CMC Tween[®]20 were relatively constant at approximately 0.7 with an increase to 0.9 at 0.05 wt% which then remained constant until 0.1 wt%. Adding 2 CMC Tween[®]20 did not produce any significant changes in sedimentation, with slightly higher sedimentation ratios found in the 0.5 CMC Tween[®]20 brine-surfactant-SiO₂ nanofluids. The evaluation of the stability of nanofluids conducted using direct visual observations of the nanoparticles in the brine-surfactant systems at different time intervals after sonication of each set of nanofluids (0,

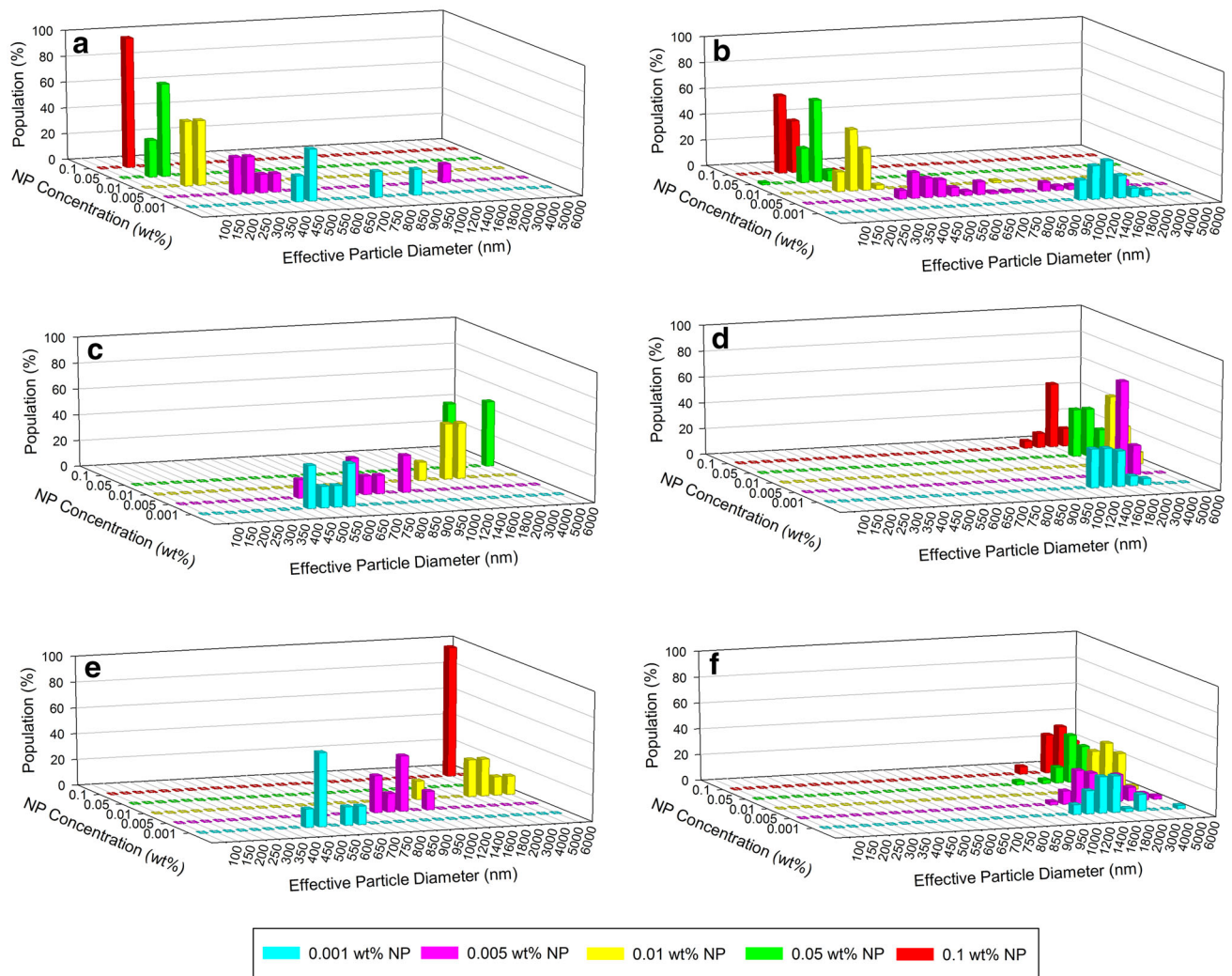


Fig. 3 Histograms of size distribution of SiO₂ nanoparticles built from dynamic light scattering measurements for five SiO₂ nanoparticle concentrations (0.001 wt% NP, 0.005 wt% NP, 0.01 wt% NP, 0.05 wt% NP, and 0.1 wt% NP), in: **a** brine-SiO₂ NP systems within 1 min; **b** brine-SiO₂ NP systems at 20–30 min; **c** brine-0.5 CMC Tween[®]20-SiO₂ NP systems within 1 min; **d** brine-0.5 CMC Tween[®]20-SiO₂ NP systems at 20–30 min; **e** brine-2 CMC Tween[®]20-SiO₂ NP systems within 1 min; **f** brine-2 CMC Tween[®]20-SiO₂ NP systems at 20–30 min

20, and 30 min) support the sedimentation results and the stability of the nanofluids (Table 3).

Surface tension of nanofluids

The surface tension of 15 nanofluids with increasing SiO₂ NPs concentration from 0.001 to 0.1 wt% is shown in Fig. 6 for all three surfactant concentrations of 0 CMC, 0.5 CMC, and 2 CMC. In the absence of Tween[®]20, the surface tension for the nanofluids increased from 61 mN/m at 0.001 wt% SiO₂ NPs to 72 mN/m at 0.1 wt% SiO₂ NPs during the initial stage; after 20 min, the values for the 0.001 wt% and 0.01 wt% increased from 65 mN/m to 76 mN/m, respectively. At a SiO₂ NPs concentration of 0.1

wt%, the surface tension decreased to 66 mN/m. After adding 0.5 CMC surfactant, the initial surface tensions for the 0.001 and 0.1 wt% brine-surfactant-SiO₂ nanofluids increased from 41 to 52 mN/m, and at equilibrium stage, the values increased from 35 to 45 mN/m. With surfactant concentrations as high as 2 CMC, the initial stage surface tensions of the brine-surfactant-SiO₂ nanofluids ranged from 37 to 46 mN/m. Over 20 min, the surface tensions were 47, 33, 42, 35, and 40 mN/m corresponding to brine-surfactant-SiO₂ nanofluids with nanoparticle concentration between 0.001 and 0.1 wt%, respectively. Average values of surface tension of crude oils measured over 30 min were 26.50 mN/m for West Texas Intermediate, 29.45 mN/m for Prudhoe Bay, and 29.25 mN/m for Lloydminster.

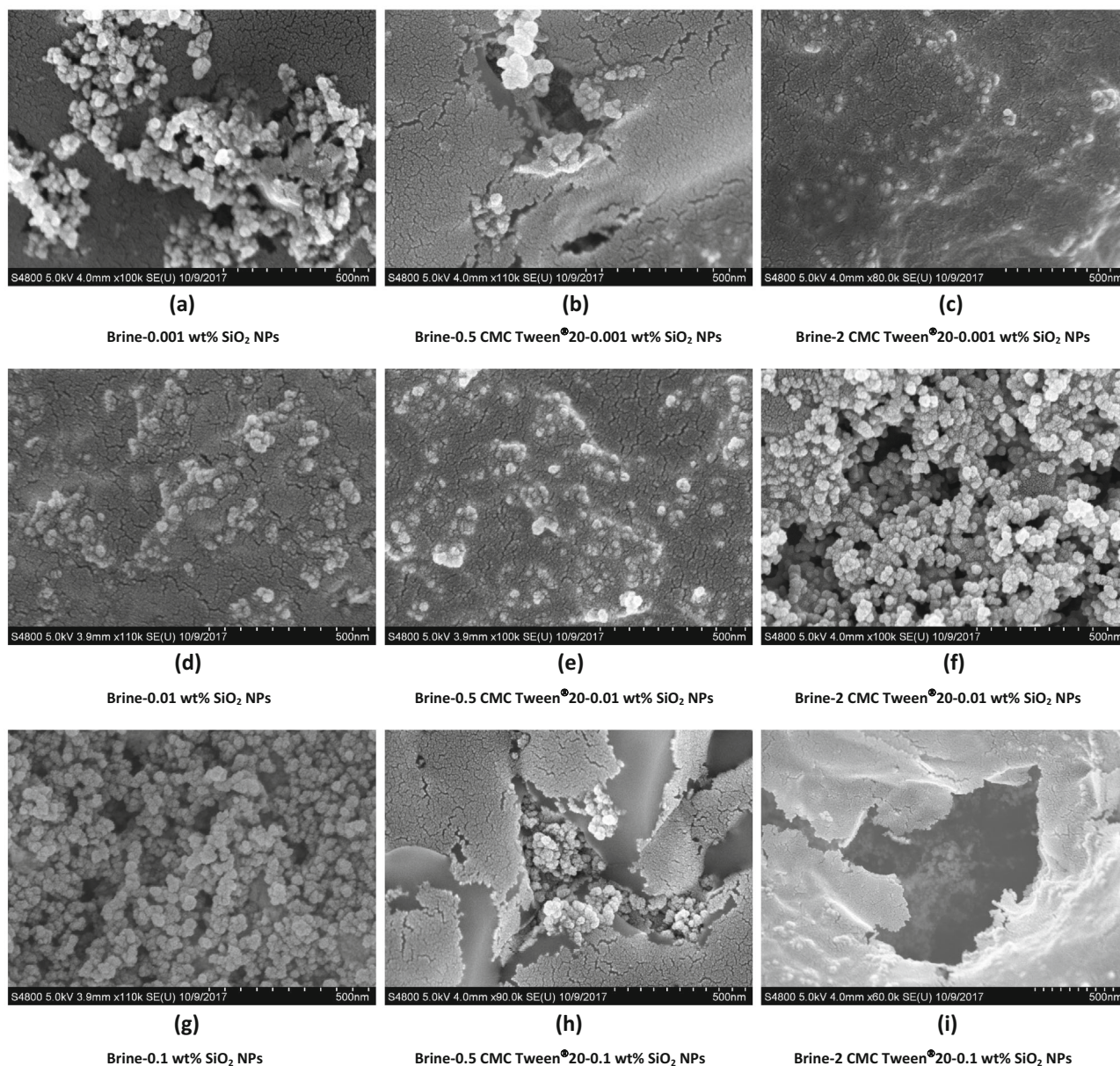


Fig. 4 SEM images of SiO₂ nanoparticles for: **a** brine-0.001 wt% SiO₂ NPs; **b** brine-0.5 CMC Tween[®]20-0.001 wt% SiO₂ NPs; **c** brine-2 CMC Tween[®]20-0.001 wt% SiO₂ NPs; **d** brine-0.01 wt% SiO₂ NPs; **e** brine-0.5 CMC Tween[®]20-0.01 wt% SiO₂ NPs; **f** brine-2 CMC

Tween[®]20-0.01 wt% SiO₂ NPs; **g** brine-0.1 wt% SiO₂ NPs; **h** brine-0.5 CMC Tween[®]20-0.1 wt% SiO₂ NPs; **i** brine-2 CMC Tween[®]20-0.1 wt% SiO₂ NPs

Interfacial tension between brine-surfactant-SiO₂ NPs systems and crude oils

Light crude oil

The visual observation of the interface between brine-surfactant-SiO₂ NPs systems and drops of West Texas Intermediate light crude oil are shown in Table 4. The IFT between brine-SiO₂ NPs systems and a light crude oil, West Texas Intermediate crude oil, as a function of time is shown in Fig. 7a. A smoothing function based on a Loess

Model in R to remove the outliers from Fig. 7a was then used to generate Fig. 7b. A dynamic influence of time on IFT was observed in all systems. The monitoring of the IFTs between brine-SiO₂ NPs systems and West Texas Intermediate as a function of time indicated a decrease in IFT. The IFT curve first showed a sharp decrease with values decreasing from 18.54–21.87 mN/m to 14.10–15.64 mN/m. A plateau was then observed with values remaining stable at 14.10–15.64 mN/m, indicating that the IFT stabilized and reached the equilibrium stage after the pivot time. The reference IFT of the brine-oil system (0 wt%

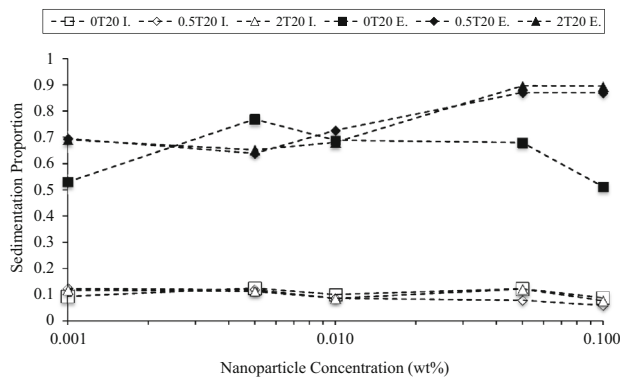


Fig. 5 Initial (I.) (open symbols) and equilibrium (E.) (solid symbols) behaviors of the sedimentation proportion of brine-SiO₂ nanofluids with five SiO₂ nanoparticle concentrations (0.001 wt% NP, 0.005 wt% NP, 0.01 wt% NP, 0.05 wt% NP, and 0.1 wt% NP) without Tween[®]20 (square symbols), in the presence of 0.5 CMC Tween[®]20 (diamond symbols), and in the presence of 2 CMC Tween[®]20 (triangle symbols)

SiO₂ NPs) at equilibrium was 14.35 mN/m, with the SiO₂ NP concentrations exhibiting a slight effect of the IFT of the brine-oil systems. The addition of SiO₂ NPs exhibited the opposite effects on the equilibrium IFT values, which depend upon the concentration of SiO₂ NPs in the nanofluid-oil systems compared to the concentration of the reference. The SiO₂ NPs concentrations of 0.001 and 0.01 wt% had slightly decreased IFT values of 14.10 and 14.22 mN/m, respectively, while the SiO₂ NP concentrations of 0.005, 0.05, and 0.1 wt% resulted in small increases in IFT, with values reaching 14.47, 15.19, and 15.64 mN/m, respectively.

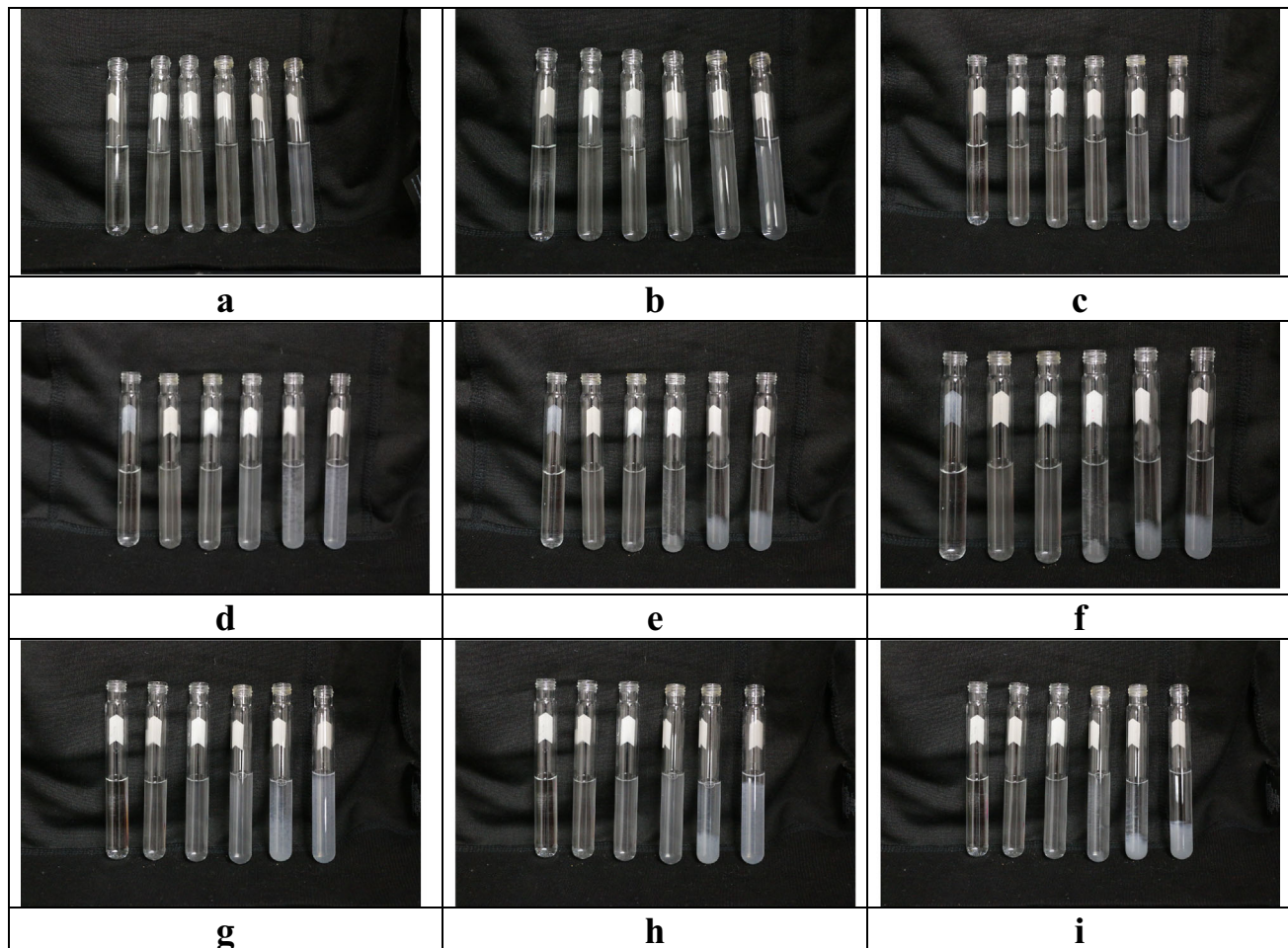
The IFT dynamics between the brine-surfactant-SiO₂ NP systems and West Texas Intermediate crude oil in the presence of Tween[®]20 at 0.5 and 2 CMC, respectively, is shown in Fig. 7c, e. The processed data using a smooth functioning on the Loess Model in R is shown in Fig. 7d, f. A similar dynamic trend was observed for the IFT of the brine-surfactant-SiO₂ nanofluid-oil systems as in the systems where surfactant was absent. IFT values decreased rapidly and then reached a plateau. The Initial IFT values for the brine-surfactant-SiO₂ nanofluid-oil systems with Tween[®]20 at 0.5 and 2 CMC fell within a range of 7.06 to 18.20 mN/m and from 8.82 to 13.86 mN/m, respectively, with the lowest IFT values occurring for 0 wt% SiO₂ NP. The presence of Tween[®]20 at 0.5 and 2 CMC significantly reduced the IFTs between the oil and brine-surfactant and the oil and brine-surfactant SiO₂ NPs compared to the same systems without surfactant. However, the concentration of SiO₂ NPs did affect the IFT of these systems. Specifically an increase in the SiO₂ NPs concentration in the brine-surfactant-SiO₂ nanofluid-oil systems caused a corresponding increase in the IFT of these systems at equilibrium (Fig. 8). The average IFT values at equilibrium

ranged from 3.97 mN/m (0 wt% SiO₂ NP) to 9.42 mN/m (0.1 wt% SiO₂ NPs), and 4.22 mN/m (0 wt% SiO₂ NP) to 12.73 mN/m (0.1 wt% SiO₂ NPs) for brine-surfactant-SiO₂ nanofluid-oil systems with Tween[®]20 at 0.5 and 2 CMC, respectively; the lowest IFT values for the 0.5 and 2 CMC Tween[®]20 systems occurred for those without nanoparticles (0 wt% SiO₂ NP).

Medium crude oil

The visual observation of the interface between brine-surfactant-SiO₂ NPs systems and drops of Prudhoe Bay medium crude oil are shown in Table 5. The IFT dynamics between SiO₂ NPs systems and Prudhoe Bay medium crude oil is shown in Fig. 9a, and the processed data, developed with a smoothing function based on a Loess Model in R, is shown in Fig. 9b. The dynamic change trend in IFT varies with that of the SiO₂ NP concentration. The reference IFT of the brine-oil system remained quite stable over time with an initial IFT of 17.55 mN/m and equilibrium IFT of 18.25 mN/m. However, the addition of SiO₂ NPs to the brine resulted in a significant decrease in all IFTs between the brine-SiO₂ NP systems and Prudhoe Bay crude oil, regardless of the SiO₂ NP concentration. The SiO₂ NP concentrations of 0.005 and 0.05 wt% stabilized the IFTs over time, with equilibrium IFTs of 13.16 and 13.11 mN/m, respectively. The SiO₂ NP concentrations of 0.001, 0.01 and 0.1 wt% showed a decrease in IFT values over time, with the lowest IFT value occurring at equilibrium 10.40 mN/m with an SiO₂ NP level of 0.001 wt%.

The IFT dynamics between brine-surfactant-SiO₂ NPs systems and Prudhoe Bay crude oil is shown in Fig. 9c, e. The processed data, developed from a smoothing function based on the Loess Model in R in the presence of Tween[®]20 at 0.5 CMC and 2 CMC, is shown in Fig. 9d, f. The IFT dynamics between brine-surfactant-SiO₂ NPs systems and Prudhoe Bay crude oil showed two trends depending on the concentration of SiO₂ NPs. The initial IFTs values ranged from 9.73 to 17.59 mN/m and from 8.01 to 13.58 mN/m. With Tween[®]20 at 0.5 CMC, the SiO₂ NP concentrations of 0 wt%, and 0.01 wt% induced a decrease in IFT to reach equilibrium. The lowest equilibrium IFT value, 5.45 mN/m, for the brine-surfactant-SiO₂ NPs systems and Prudhoe Bay crude oil for Tween[®]20 at 0.5 CMC was obtained with 0.001 wt%, while for Tween[®]20 at 2 CMC it was achieved with 0.005 wt% of SiO₂ NPs, which was 5.81 mN/m. The 0.05 wt% concentration with Tween[®]20 at 0.5 CMC induced an increase in IFTs with equilibrium values reaching 16.40 mN/m. All six SiO₂ NPs concentrations with Tween[®]20 at 2 CMC induced significant decreases in IFT over time, especially the 0.05 wt% concentration with Tween[®]20 at 2 CMC,

Table 3 Visual observation of nanofluid systems stability

Images of nanofluids at 0 min (a), 20 min (b), 30 min (c) after sonication of the set of nanofluids: From left to right are 0 wt%, 0.001 wt%, 0.005 wt%, 0.01 wt%, 0.05 wt%, 0.1 wt% nanoparticle suspensions with 5 wt% brine, respectively. Images of nanofluids at 0 min (d), 20 min (e), 30 min (f) after sonication of the set of nanofluids: From left to right are 0 wt%, 0.001 wt%, 0.005 wt%, 0.01 wt%, 0.05 wt%, 0.1 wt% nanofluids with 5 wt% brine and 0.5 CMC Tween[®] 20, respectively. Images of nanofluids at 0 min (g), 20 min (h), 30 min (i) after sonication of the set of nanofluids: From left to right; 0 wt%, 0.001 wt%, 0.005 wt%, 0.01 wt%, 0.05 wt%, 0.1 wt% nanofluids with 5 wt% brine and 2 CMC Tween[®] 20, respectively

which kept decreasing IFT after the initial 30 min. Except for the SiO₂ NP concentrations at 0.005 wt% with 2 CMC Tween[®] 20 that yielded a minimal IFT at equilibrium, an increase in the SiO₂ NP concentrations in the brine-surfactant-SiO₂ nanofluid-oil systems was observed with a corresponding increase in the IFT at equilibrium (Fig. 10). In the presence of surfactant, the maximum IFTs were obtained with the highest SiO₂ NPs concentration (0.1 wt%), while without surfactant, the maximum IFT was obtained without the addition of SiO₂ NPs. Also, as the SiO₂ NP concentrations increased, the equilibrium IFT values with Tween[®] 20 at 2 CMC became larger than that obtained with Tween[®] 20 at 0.5 CMC.

Heavy crude oil

The visual observation of the interface between brine-surfactant-SiO₂ NPs systems and drops of Lloydminster heavy crude oil are shown in Table 6. The IFT dynamics between the brine-SiO₂ NP systems and Lloydminster heavy crude oil is shown in Fig. 11a, and the processed data using a smoothing function based on the Loess Model in R is shown in Fig. 11b. A similar IFT trend was observed for all the SiO₂ NP concentrations. A variance in the IFTs between the SiO₂ NP systems and the Lloydminster crude oil occurred over time with a sharp increase and a plateau as the IFT reaches equilibrium. These IFTs were also influenced by SiO₂ NPs concentrations with initial IFT

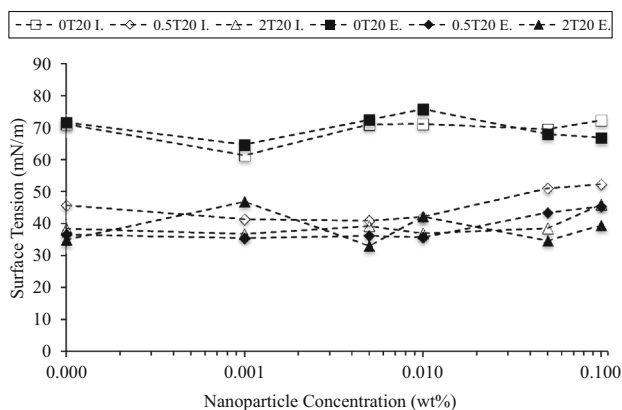


Fig. 6 Initial (I.) (open symbols) and equilibrium (E.) (solid symbols) behaviors of the surface tension for brine-SiO₂ nanofluids with five different SiO₂ nanoparticle concentrations (0.001 wt% NP, 0.005 wt% NP, 0.01 wt% NP, 0.05 wt% NP, and 0.1 wt% NP) without Tween[®]20 (square symbols), in the presence of 0.5 CMC Tween[®]20 (diamond symbols), and in the presence of 2 CMC Tween[®]20 (triangle symbols)

values ranging from 4.30 to 16.29 mN/m. An increase in the concentration of SiO₂ NPs resulted in a corresponding decrease in the IFT values of SiO₂ NPs at equilibrium, from 21.81 mN/m for 0.001 wt% to 14.19 mN/m for 0.1

wt%. All of the SiO₂ nanofluid systems showed an increase in the IFT dynamics over time. The reference equilibrium IFT obtained in the brine solution without SiO₂ NPs (0 wt% SiO₂ NP) was 18.62 mN/m.

The IFT dynamics between the brine-surfactant-SiO₂ NP systems and Lloydminster crude oil in the presence of Tween[®]20 at 0.5 CMC and 2 CMC is shown in Fig. 11c, e. The processed data developed from a smoothing function based on the Loess Model in R is shown in Fig. 11d, f. The IFT dynamics between the brine-surfactant-SiO₂ NPs systems and the Lloydminster crude oil sample exhibited two separate values with the use of the Tween[®]20 at a 0.5 CMC: an initial IFT value range of 6.37 to 11.40 mN/m, and SiO₂ NP concentrations of 0 to 0.001 wt%. A sharp increase in the IFT was observed prior to the occurrence of a similar IFT equilibrium of approximately 11 mN/m, which was the lowest obtained from the brine-surfactant-SiO₂ NPs system. The remaining SiO₂ NPs concentrations (0.005, 0.01, 0.05, and 0.1 wt%) resulted in a sharp increase in the IFT to reach equilibrium. The highest equilibrium IFT values for brine-surfactant-SiO₂ NPs systems and the Lloydminster crude oil sample was 16.44 mN/m for Tween[®]20 at 0.5 CMC, which was obtained with 0.05 wt% SiO₂ NPs. For Tween[®]20 at 2

Table 4 Visual observation of the interface between brine-surfactant-SiO₂ NPs systems and drops of West Texas Intermediate light crude oil

Nanoparticle Concentrations	Brine and Surfactant Concentrations					
	5 wt% Brine		5 wt% Brine + 0.5 CMC Tween [®] 20		5 wt% Brine + 2 CMC Tween [®] 20	
	1 min	20 min	1 min	20 min	1 min	20 min
0 wt% SiO ₂						
0.001 wt% SiO ₂						
0.005 wt% SiO ₂						
0.01 wt% SiO ₂						
0.05 wt% SiO ₂						
0.1 wt% SiO ₂						

Representative drops images of West Texas Intermediate light crude oil at both the initial and equilibrium phases in brine-surfactant-SiO₂ NPs systems

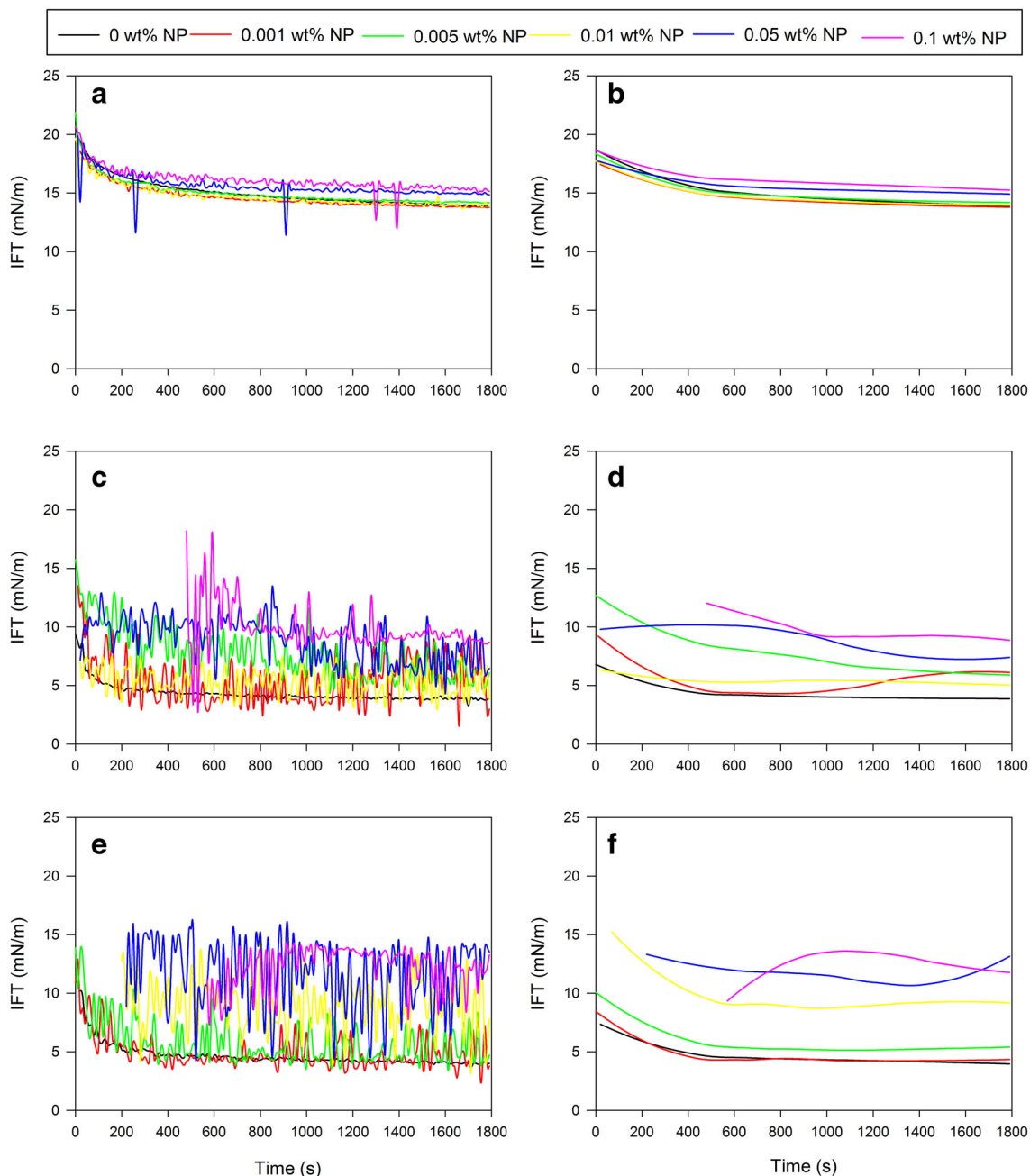


Fig. 7 Dynamic IFTs between brine-surfactant-SiO₂ nanofluids and West Texas Intermediate light crude oil with different mass fractions of SiO₂ nanoparticles (0.001 wt% NP, 0.005 wt% NP, 0.01 wt% NP, 0.05 wt% NP, and 0.1 wt% NP) without Tween[®]20 (0 CMC): **a** raw

data, and **b** processed data in Loess Model in R; in the presence of 0.5 CMC Tween[®]20: **c** raw data, and **d** processed data in Loess Model in R; and in the presence of 2 CMC Tween[®]20: **e** raw data, and **f** processed data in the Loess Model in R

CMC, the IFT dynamics between the brine-surfactant-SiO₂ NP systems and the Lloydminster crude oil showed an oscillating change in IFT with time. Initial IFT values fell within a range of 7.15 to 18.79 mN/m, with the highest IFT equilibrium achieved at 19.55 mN/m obtained with 0.1 wt% SiO₂ NPs, and the lowest at 8.70 with 0.001 wt%.

As shown in Fig. 12, the equilibrium IFTs of the brine-SiO₂ nanofluid oil systems are higher than those produced

with the surfactant, except for the highest concentrations of SiO₂ NPs. Also, an increase in the SiO₂ NP concentration generally resulted in a corresponding increase of the equilibrium of the IFT brine-surfactant-SiO₂ nanofluid-oil systems, while a decrease of equilibrium IFT was generally observed with the brine-SiO₂ nanofluid-oil systems.

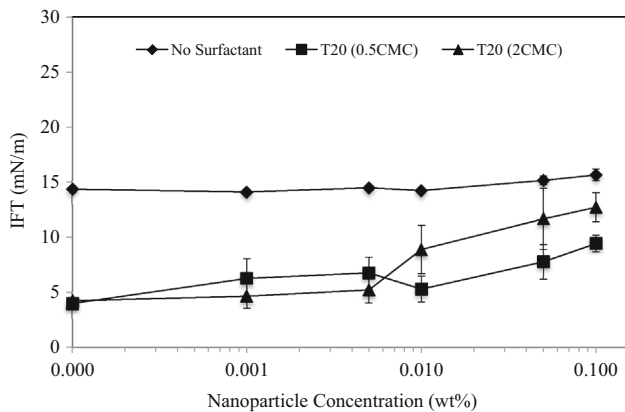


Fig. 8 Equilibrium IFTs between brine-SiO₂ nanofluids and West Texas Intermediate light crude oil with different mass fractions of SiO₂ nanoparticles (0.001 wt% NP, 0.005 wt% NP, 0.01 wt% NP, 0.05 wt% NP, and 0.1 wt% NP) without surfactant (diamond symbols) in the presence of 0.5 CMC Tween[®]20 (square symbols) and 2 CMC Tween[®]20 (triangle symbols)

Discussion

Stability of SiO₂ based nanofluids

The stability of nanofluids is defined by the extent to which SiO₂ NPs remain in suspension over time. The stability of

our nanofluid suspensions was examined via the analyses of size, zeta potential, and sedimentation rates of SiO₂ NPs. The high surface free energy of SiO₂ NPs often causes the formation of large nanoaggregates that cannot remain in suspension (Ganguly and Chakraborty 2011). When the SiO₂ NPs leave suspension, they cannot connect at the liquid–liquid interface and alter the IFT. The size of the SiO₂ nanoaggregates establishes the possibility of settling due to the aggregation phenomenon, leaving smaller stable nanoaggregates the possibility of affecting the IFT. In SiO₂ NPs concentrations of 0.001 and 0.1 wt%, the SiO₂ NPs aggregated to 1503 ± 289 and 249 ± 12 nm diameter particles, respectively, in a 5% brine solution. An increasing concentration of NPs in brine reduced the size of nanoaggregates, due to the settling of the larger nanoaggregates formed at higher concentrations of NPs, thus leaving the smaller nanoaggregates in suspension. The addition of 0.5 CMC of surfactant increased the SiO₂ nanoaggregate diameters to 1593 ± 282 and 2951 ± 1033 nm at 0.001 and 0.1 wt% concentrations respectively. The addition of surfactant was added to the systems at 2 CMC increased the nanoaggregate diameters to 1680 ± 648 and 3475 ± 1099 nm at concentrations of 0.001 and 0.1 wt% respectively. In these suspensions, higher SiO₂ NPs concentrations produced nanoparticle-

Table 5 Visual observation of the interface between brine-surfactant-SiO₂ NPs systems and drops of Prudhoe Bay medium crude oil

Nanoparticle Concentrations	Brine and Surfactant Concentrations					
	5 wt% Brine		5 wt% Brine + 0.5 CMC Tween [®] 20		5 wt% Brine + 2 CMC Tween [®] 20	
	1 min	20 min	1 min	20 min	1 min	20 min
0 wt% SiO ₂						
0.001 wt% SiO ₂						
0.005 wt% SiO ₂						
0.01 wt% SiO ₂						
0.05 wt% SiO ₂						
0.1 wt% SiO ₂						

Representative drop images of Prudhoe Bay medium crude oil at initial and equilibrium phases in brine-surfactant-SiO₂ NPs systems

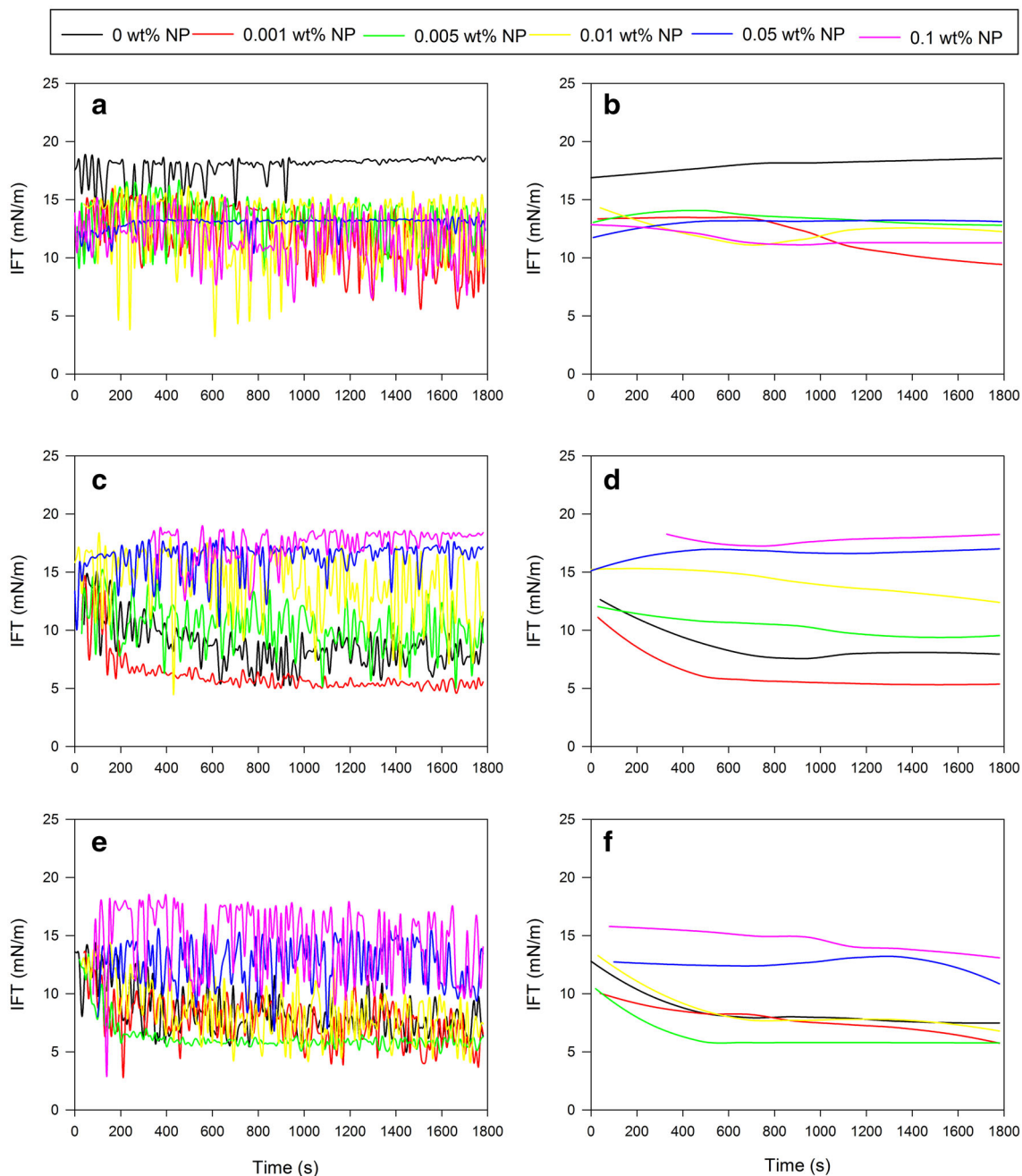


Fig. 9 Dynamic IFTs between brine-surfactant-SiO₂ nanofluids and Prudhoe Bay medium crude oil with different mass fractions of SiO₂ nanoparticles (0.001 wt% NP, 0.005 wt% NP, 0.01 wt% NP, 0.05 wt% NP, and 0.1 wt% NP) without Tween[®]20 (0 CMC): **a** raw data,

and **b** processed data in Loess Model in R; in the presence of 0.5 CMC Tween[®]20: **c** raw data, and **d** processed data in Loess Model in R; and in the presence of 2 CMC Tween[®]20: **e** raw data, and **f** processed data in the Loess Model in R

surfactant complexes and removed the surfactant from the bulk solution. The surfactant in turn affected the interactions between the nanoparticles by increasing repulsion forces between the SiO₂ NPs. The lack of surfactant at higher SiO₂ NPs concentrations indicates that the SiO₂ NPs produced larger SiO₂ nanoaggregates with larger-than-suitable diameters (Cieslinski and Krygier 2014; Ehtesabi et al. 2014). The smaller diameters of nanoaggregates

reported in previous findings were most likely the consequence of longer sonication times which yielded a more thorough mixture of the NPs into the suspension. Furthermore, unlike similar studies detailing various nanoaggregates, we used a higher concentration of 5% brine to generate higher aggregation rates and larger nanoaggregate sizes (Ehtesabi et al. 2014; Hendraningrat and Torsæter 2014). This variance in brine characteristics may serve as a

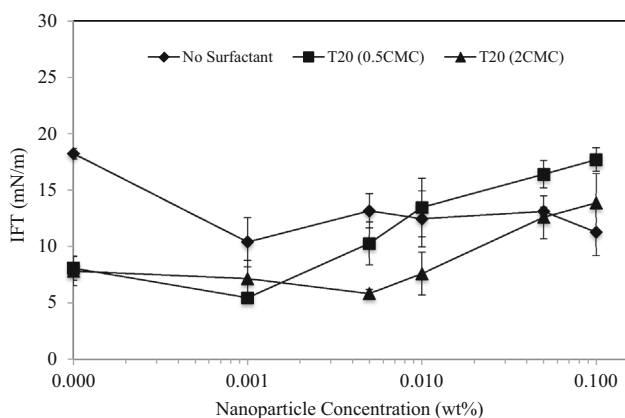


Fig. 10 Equilibrium IFTs between brine-SiO₂ nanofluids and Prudhoe Bay medium crude oil with different mass fractions of SiO₂ nanoparticles (0.001 wt% NP, 0.005 wt% NP, 0.01 wt% NP, 0.05 wt% NP, and 0.1 wt% NP) without surfactant (diamond symbols) in the presence of 0.5 CMC Tween[®]20 (square symbols) and 2 CMC Tween[®]20 (triangle symbols)

possible explanation for the larger size of nanoaggregates detected in our study in which the large standard deviations observed for the nanoaggregate size indicate a high degree of polydispersity of the nanofluids. However, further research should be conducted in the development of smaller nanoaggregates for purposes of increasing the

stability of the brine-surfactant-SiO₂ nanofluid systems and ensure the optimum migration of SiO₂ NPs and surfactant to the oil-aqueous interface for a maximum potential impact on IFT.

The influence of the SiO₂ NPs size distribution on the stability of SiO₂ NPs was revealed. In the brine-SiO₂ NP systems, the lower SiO₂ NP concentrations of 0.001 and 0.005 wt% showed a polydisperse size distribution and resulted in the formation of larger SiO₂ NP aggregates than higher concentration of SiO₂ NPs that tended to be monodispersed. In the brine-Tween[®]20-SiO₂ NP systems, the lower SiO₂ NP concentrations of 0.001 and 0.005 wt% generated the smallest sizes of SiO₂ NP aggregates. This may be attributed to the combining effects of the polydisperse size distribution of SiO₂ NPs and the surfactant that limits the aggregation phenomena.

The zeta potential values observed for the majority of the nanofluid systems were close to zero, an indication of the low degree of stability of the systems, a stability that can be increased by the addition of a surfactant (Fig. 2a, b, c) (Zargartalebi et al. 2014). The adsorption of surfactants onto nanoparticles eventually triggers a steric repulsion on the SiO₂ NPs, which in conjunction with the electrostatic forces of the SiO₂ NPs promotes suspension stability. The larger size of SiO₂ nanoaggregates measured with the

Table 6 Visual observation of the interface between brine-surfactant-SiO₂ NPs systems and drops of Lloydminster heavy crude oil

Nanoparticle Concentrations	Brine and Surfactant Concentrations					
	5 wt% Brine		5 wt% Brine + 0.5 CMC Tween [®] 20		5 wt% Brine + 2 CMC Tween [®] 20	
	1 min	20 min	1 min	20 min	1 min	20 min
0 wt% SiO ₂						
0.001 wt% SiO ₂						
0.005 wt% SiO ₂						
0.01 wt% SiO ₂						
0.05 wt% SiO ₂						
0.1 wt% SiO ₂						

Representative drop images of Lloydminster heavy crude oil at initial and equilibrium phases in brine-surfactant-SiO₂ NPs systems

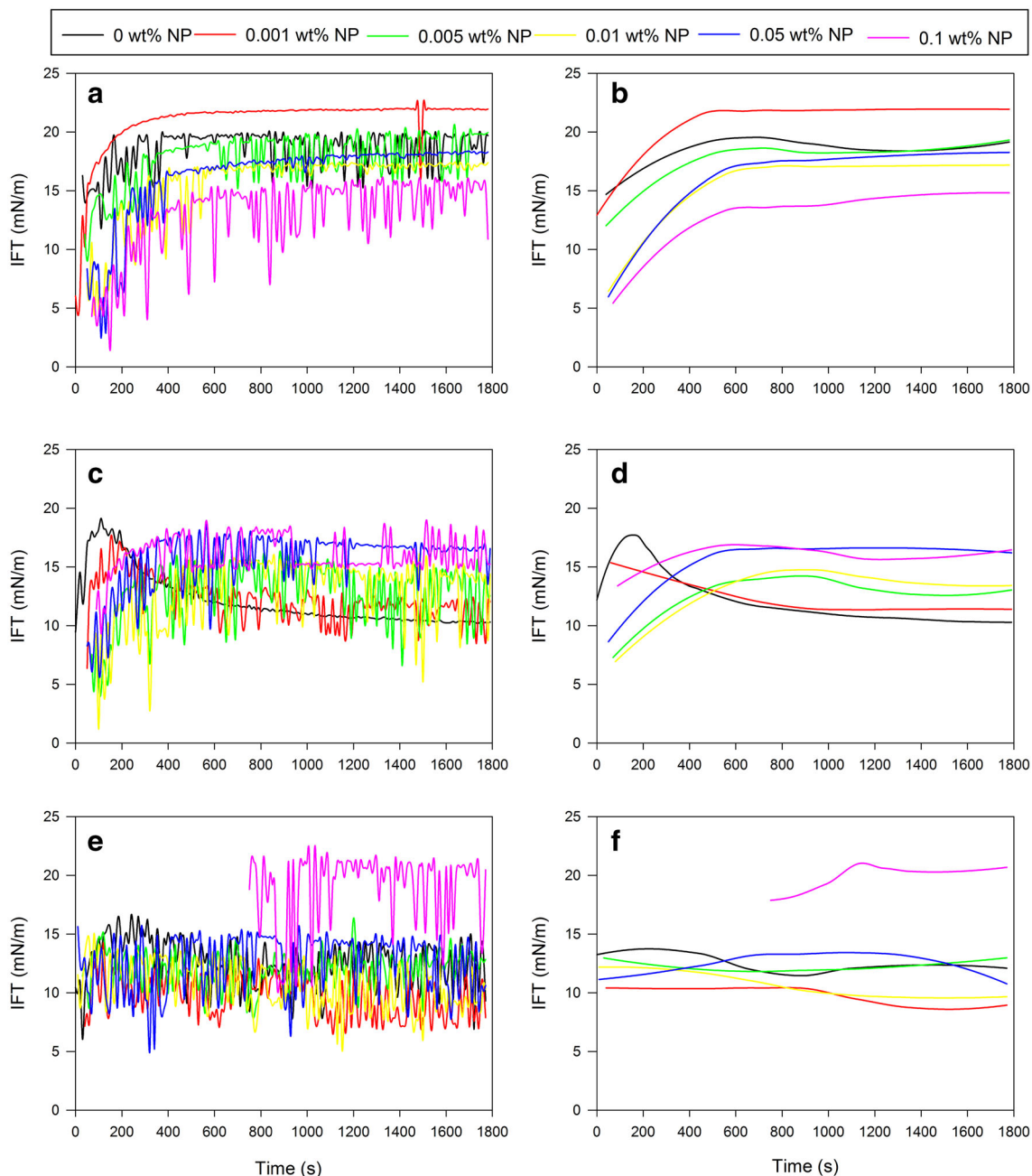


Fig. 11 Dynamic IFTs between brine-surfactant-SiO₂ nanofluids and Lloydminster heavy crude oil with different mass fractions of SiO₂ nanoparticles (0.001 wt% NP, 0.005 wt% NP, 0.01 wt% NP, 0.05 wt% NP, and 0.1 wt% NP) without Tween[®]20 (0 CMC): **a** raw data,

and **b** processed data in Loess Model in R; in the presence of 0.5 CMC Tween[®]20: **c** raw data, and **d** processed data in Loess Model in R; and in the presence of 2 CMC Tween[®]20: **e** raw data, and **f** processed data in the Loess Model in R

addition of the nonionic surfactant, Tween[®]20, indicated the creation of these surfactant-nanoparticle complexes that remained in suspension. The largest zeta potential among the systems was -11 ± 38 mV in a brine with 0.001 wt% NPs, whereas the corresponding zeta potential for the identical system with a surfactant was only 9 ± 32 mV at 0.5 CMC and 6 ± 41 mV at 2 CMC. The relatively large standard deviation between measurements derived mostly

from the positive and negative measurements recorded for the samples.

As observed in our study, the sedimentation rate of the nanofluid systems strongly supports the previously established association of the nanoaggregate size with that of the sedimentation rate (Cieslinski and Krygier 2014). In our study, a settling of the NPs from the solutions to almost half their initial concentration was observed after a 30 min

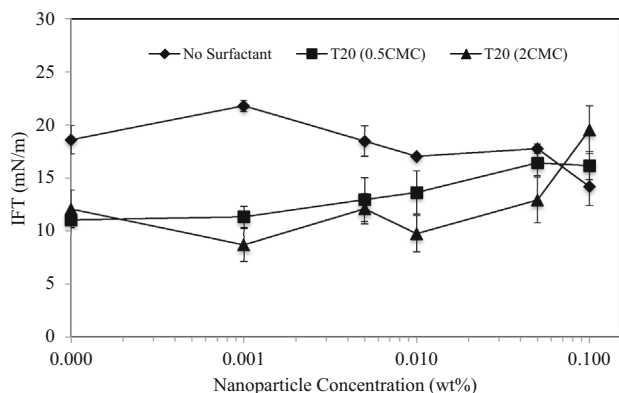


Fig. 12 Equilibrium IFTs between brine-SiO₂ nanofluids and Lloydminster heavy crude oil with different mass fractions of SiO₂ nanoparticles (0.001 wt% NP, 0.005 wt% NP, 0.01 wt% NP, 0.05 wt% NP, and 0.1 wt% NP) without surfactant (diamond symbols) in the presence of 0.5 CMC Tween[®]20 (square symbols) and 2 CMC Tween[®]20 (triangle symbols)

period. The lowest sedimentation proportion occurred within a NP brine solution of 0.001 wt% with a lower relative concentration of 0.53 ± 0.01 , a behavior that reflected the size of the nanoaggregates in a 0.001 wt% solution. The larger size of these nanoaggregates was due to the lack of settling that is so characteristic in low SiO₂ NP concentrations. The opposite behavior, however, remained valid for the brine and surfactant system as the nanoparticle-surfactant complexes retain the nanoaggregates in suspension, even with an increase in the nanoaggregate size.

Raspberry-like morphology of SiO₂ nanoparticles

SEM confirms the raspberry-like morphology particles of these assemblages of SiO₂ nanoparticles (Fig. 4). The roughness of the coating provided by the raspberry-like morphology particles is critical for the wetting properties of these SiO₂ nanofluid systems (Carcouet 2014; Carcouet et al. 2014; Fan et al. 2012; Yu et al. 2017; Zanini et al. 2017). The formation of these raspberry-like particles in brine-SiO₂ NP systems, with high surface area, may be attributed to the aggregation and self-assembly capabilities of SiO₂ NPs induced by the salt concentration (i.e., 5 wt% NaCl) (Uzelac et al. 2017). The coupling of the physico-chemical properties of the SiO₂ nanoparticles and Tween[®]20 surfactant have proven to be very effective in altering the interfacial process in oil-SiO₂ nanofluid systems (i.e., the decrease of the interfacial tension of oil-SiO₂ nanofluid systems) under synergistic effects of SiO₂ NP and surfactant concentrations and as a function of the crude oil properties. SEM images of the hybrid particles of Tween[®]20/SiO₂ confirm that the raspberry-like morphology was gained directly from the polymerization of the

SiO₂-stabilized nanoparticles. Similar raspberry-like morphology nanostructures have been previously also reported with metalloids nanoparticles (e.g., silicon dioxide nanoparticles) and metal nanoparticles (e.g., iron oxide nanoparticles) (Hu et al. 2016b; Kresge et al. 1992; Roosz et al. 2017; Stauch et al. 2017; Uzelac et al. 2017; Zanini et al. 2017; Zhao and Middelberg 2013). The effects of surfactant and salt electrolyte on the morphology of the self-assembled particles (brine-SiO₂ NP systems) and self-assembled polymer composites were also visualized. It has been previously demonstrated that the coverage of the raspberry-like particle increases with increasing salt concentration (Meeusen 2017). Our results support these findings as a high coverage of the raspberry-like particles was observed with a high NaCl-based brine concentration of 5 wt% for the Tween[®]20-SiO₂ NP systems. The development of this raspberry-like particles material with high surface area, high salt stability, and high capability of interfaces alteration and therefore wettability changes offers a wide range of applications in the fields of applied nanoscience, environmental engineering, and petroleum engineering.

Effects of SiO₂ nanoparticles concentration and surfactant concentration on the dynamic and equilibrium interfacial tension at the oil-aqueous interface for brine-surfactant-SiO₂ nanofluid-oil systems

Altering the IFT at the oil-aqueous interface in a reservoir is necessary for generating the mobility and recovery of both the oil that is trapped within the small pores of the geologic formations and the residual oil that remains within the pores after the secondary recovery phase (Roustaei and Bagherzadeh 2013, 2015; Joonaki and Ghanaatian 2014; Yuan et al. 2015; Hu et al. 2016a; Pu et al. 2016). The wettability of an oil reservoir is dependent on the conditions that exist at the pore interfaces, conditions which govern the stability and movement of the interfaces and the resulting oil migration. In traditional reservoir exploitation under original wetting conditions, i.e. water-wet conditions before any oil migration, the decrease of IFT will induce a decrease in capillary pressure in the pores which results in the mobilization of both the trapped and residual oil. With an extreme change in wettability such as in the wettability reversal of a reservoir to a water-wet condition, a central process of EOR, an increase in IFT will lead to increasing capillary pressures that will result in an increased wettability of the pores, and a strong imbibition of the wetting phase into the small pores which will thus enhance the oil recovery (Yu et al. 2008). In our study on the effects of SiO₂ nanoparticles on IFT of brine-surfactant-crude oil systems, we determined that these nanoparticles either

decrease IFT, increase IFT, or exhibit no affect at all. Clearly, the constituents of these oil and aqueous substances do indeed affect the IFT behavior of brine-surfactant-crude oil systems, with the presence of nanoparticles leading to these contrasting IFT trends according to the type of crude oil.

Our study also demonstrates the effect of SiO₂ NPs on interfaces in crude oil-surfactant-brine systems with diverse behaviors at these interfaces that were dependent on the physico-chemical of the oil, and the concentrations of both NPs and surfactants. Changes in the oil-aqueous phase IFT were observed in the presence of nonionic surfactant as a result of adding SiO₂ NPs to the aqueous phase, as also observed by Eskandar et al. (2007) and Wang et al. (2004). For most oils, in the absence of nonionic surfactant, no significant change in oil–water IFT was detected with the addition of approximately 0.1 wt% of SiO₂ NPs. In the presence of 0.5 and 2 CMC Tween[®]20, the IFT of the different systems either increased or decreased as a function of the concentration of SiO₂ NPs. In terms of the IFT trends, however, a threshold concentration of SiO₂ NPs was observed for the medium (0.5 and 2 CMC) and heavy (2 CMC) oil systems. Concentrations above and below this SiO₂ NPs threshold concentration resulted in a respective increase and decrease, with the latter caused by the spontaneous self-assembly of surfactant or SiO₂ NPs at liquid–liquid interfaces, which are a central component in EOR (Biswal and Singh 2016). A further increase in concentration also greatly increased the IFT values to levels much greater than detected in the absence of NPs. For medium and heavy crude oil, the presence of SiO₂ NPs enhances the efficiency of nonionic surfactant molecules in decreasing the IFT. It has been established that the presence of SiO₂ NPs at the interfacial layer does cause a reduction of IFT. Specifically, at low concentrations, SiO₂ NPs attach to the liquid surface with a subsequent decrease in surface tension from adsorption (Suleimanov et al. 2011). However, at concentrations larger than 0.001 wt%, SiO₂ NPs remove the surfactant from the bulk aqueous phase, which in turn decreases the free surfactant. This phenomenon increases as the concentration of SiO₂ NPs increases, with the ultimate removal of nearly the entirety of the surfactant from the bulk phase with no free surfactant remaining in the bulk solution. The depletion of the surfactant due to adsorption on particle surfaces may also cause the increase in the oil–water IFT (Brian and Chen 1987). As shown in Figs. 10 and 12, IFTs are close to the brine system IFTs for nanoparticle concentrations larger than 0.05 wt%, indicating that the SiO₂ NPs remove the surfactant from the bulk aqueous solution, as supported by sedimentation and visual observations (Fig. 2b, c, and Table 3). Also, for SiO₂ NPs below 0.005 wt%, the IFT is controlled by a mixed layer composed of attached SiO₂ NPs and surfactant adsorbed at

liquid interfaces. No free surfactant remains above this concentration with the increase in IFT possibly attributed to the attachment of SiO₂ NPs at the interface.

The IFT of oil-aqueous systems shifts to high IFT values after the SiO₂ NP concentration reaches a threshold and increases as a function of SiO₂ NPs. In most systems, the addition of SiO₂ NPs to a surfactant in concentrations higher than a single CMC causes an increase in the IFT after the SiO₂ NP threshold concentration is reached. The equilibrium IFT of the surfactant may be affected by the adsorption of the surfactant on the particles, the depletion of the free surfactant from the interface, and the interfacial transfer of particles as surfactant carriers (Gonzenbach et al. 2006). The attachment of SiO₂ NPs at the oil–water interface, if their concentration is low, need not automatically indicate a significant change in IFT, however. Nonetheless, from this point, Tween[®]20 molecules adsorbed on SiO₂ NPs do transfer into the liquid–liquid interface. This transfer process, which can govern the decrease in IFTs, is more complex with increases in particle concentration at the oil–water interface. Either an increase or a decrease in slope above certain concentrations of SiO₂ NPs for dynamic IFTs indicates the beginning of a possible interaction of SiO₂ NPs above a certain level of coverage of the surface. In this case, particle–particle interactions can become essential and have a greater influence on IFT (e.g., increase nanoaggregate size).

Furthermore, an increase in surfactant concentration in medium and heavy oil reduces the efficacy of the SiO₂ NPs in that enough nonionic surfactant molecules are at the interface to maintain IFT at higher levels. In the case of nonionic surfactants, as more Tween[®]20 molecules migrate from the bulk phase to the interface, more surfactant molecules remain free at a higher rather than a lower CMC for the same SiO₂ NP concentration. Consequently, the IFT decreases until the NP concentrations reach a threshold, at which point the synergetic effects manifest as opposite of the antagonistic effects (Ranatunga et al. 2011; Moghadam and Azizian 2014a, b, c; Moghadam et al. 2015; Biswal and Singh 2016). Below this threshold, a synergistic effect is observed between the nonionic surfactants and SiO₂ NPs which decreases the IFT within the oil–water interfaces. The adsorption of both the SiO₂ NPs and surfactants at the individual interface also increases the IFT reduction from this synergistic effect. For SiO₂ NPs below a threshold concentration (Figs. 10 and 12), the synergistic interactions between NPs and surfactant decrease the IFT beyond that observed for individual components. Therefore, for low concentrations of SiO₂ NPs, the IFT is governed by a mixed layer comprised of attached SiO₂ NPs and the surfactant adsorbed to the liquid interface (Ravera et al. 2006, 2008; Suleimanov et al. 2011). Conversely, an antagonistic effect is detected above

this threshold level within an increase of the IFT at the oil–water interface. This synergistic/antagonistic effect is a function of the oil properties, the surfactant properties and concentrations, and the nanoparticle concentration. The concentration of SiO₂ NPs controls either the increase or decrease in IFTs, which either increases or reduces the surfactant from an oil–water interface, while the attachment energy of SiO₂ NPs is predominantly controlled by the charge and concentration of the surfactant.

The increase in the concentration of the surfactant, which results in a corresponding increase in the surface coverage of SiO₂ NPs, also causes an increase in the attraction of SiO₂ NPs to the interface of the oil–aqueous systems (Ravera et al. 2006, 2008; Zargartalebi et al. 2014). The SiO₂ NPs that are surrounded by large amounts of surfactant act as a carrier of the nonionic surfactant Tween[®]20 which migrates toward the interface of the oil–aqueous systems. Consequently, the reduction in IFT is the possible result of a surfactant release from the particles at the interface and an alteration in tension (Ahualli et al. 2011). Further, the precipitous decline in the dynamic IFT may be a result of the physical properties of SiO₂ NPs (e.g., the size) rather than the interaction between SiO₂ NPs and surfactant. A reduction in IFT may be caused by the attachment of SiO₂ NPs at the oil–aqueous interface. The hydrophobic and hydrophilic nature of the SiO₂ NPs causes a manifestation of this attachment (Ghezzi et al. 2001; Schwartz et al. 2001).

The influence of the SiO₂ NPs size distribution on the IFTs was detected for low SiO₂ NP concentrations. For SiO₂ NP concentrations of 0.001 and 0.005 wt%, larger sizes of SiO₂ NP aggregates and polydisperse size distributions of SiO₂ NPs were observed for the brine–SiO₂ NP systems. These systems induced a decrease in IFTs in the case of the medium crude oil Prudhoe Bay. For SiO₂ NP concentrations ranging from 0.001 to 0.01 wt%, smaller sizes of SiO₂ NP aggregates were formed and polydisperse size distributions of SiO₂ NPs were also observed for the brine–0.5 CMC Tween[®]20–SiO₂ NP and the brine–2 CMC Tween[®]20–SiO₂ NP systems. In the case of the medium crude oil Prudhoe Bay, these two systems also induced a decrease in IFTs, while for the heavy oil Lloydminster the largest decrease in IFT was generated by the 2 CMC Tween[®]20–0.001% SiO₂ NPs system.

Effects of SiO₂ nanoparticles on nonionic surfactant properties: interfacial and adsorption mechanisms

The interfacial behavior of nonionic surfactant in the presence of SiO₂ NPs can provide some insights concerning their interfacial and adsorption mechanisms. It is possible that the observed IFTs are a result of either (1) the depletion of surfactant solution from the adsorption of

Tween[®]20 on the particle, which thus causes an increase in IFT with an increase in nanoparticle concentration, or (2) the adsorption of NPs at the interfacial layer, which decreases the IFT (Ravera et al. 2006, 2008). In the absence of surfactant or at low surfactant concentrations, SiO₂ NPs are fully wetted in the aqueous phase and remain within the bulk solution, avoiding the interface (Ravera et al. 2006, 2008; Ahualli et al. 2011). However, the subsequent increase in the nonionic surfactant concentration results in a corresponding increase in the number of SiO₂ NPs at the interface (Ravera et al. 2006, 2008). SiO₂ NPs that are bonded to surfactant on their surface can operate as carriers of Tween[®]20 toward the interface. The decrease in IFT may be attributed to surfactant release from the SiO₂ NPs or the direct effect of surfactant-coated SiO₂ NPs on the IFT (Ahualli et al. 2011).

Furthermore, based upon thermodynamic models, the thermodynamically positive occurrence of SiO₂ NPs at the interfaces of oil–aqueous systems causes a decrease in IFT (Paunov et al. 2002). Essentially, the adsorption of SiO₂ NPs at interface reduces the energy of the brine–surfactant–SiO₂ nanofluid–oil system (Paunov et al. 2002). The adsorption of the SiO₂ NPs also modifies the entropy of these systems. As the SiO₂ NPs are transported to the interface, this movement will generate more space for the aqueous molecules and, consequently, the entropy of the brine–surfactant–SiO₂ nanofluid–oil system changes and undergoes an expansion (Dong and Johnson 2003). These phenomena serve as the catalyst for a decrease in the total free energy of the brine–surfactant–SiO₂ nanofluid–oil system (Defay and Prigoin 1966), which therefore induces the IFT of this system to decrease.

The increase of the concentration of the nonionic surfactant increases the migration of SiO₂ NPs towards the interface indicating that capillary force phenomenon is the causative factor of this increase in IFT (Dong and Johnson 2003). The location of the SiO₂ NPs at an interface causes a lateral manifestation of the capillary forces. Finally, the increased interaction between NPs from the large SiO₂ NP concentrations generates a strong capillary force at the interface that can withstand the distortion at the interface, and thus increase the IFT. Competition between SiO₂ NPs and surfactant for adsorption at the interface of oil–water system has also been reported by Pichot et al. (2012).

Effects of oil properties on interfacial tension at the oil–aqueous interface for brine–surfactant–SiO₂ nanofluid–oil systems

The ability of the SiO₂ NPs and surfactant to decrease the IFT is related to the type of crude oil, with different behaviors of IFT between oil and aqueous phase observed for the different oil types. The overall effectiveness of the

brine-surfactant-SiO₂ nanofluids in decreasing the IFT between the oil-aqueous phase in the three crude oil samples was as follows: Prudhoe Bay > Lloydminster > West Texas Intermediate. Based on the physico-chemical characteristics of the three oils examined (Table 1) and the effectiveness of the brine-surfactant-SiO₂ nanofluids in decreasing the IFT between the oil-aqueous phase that are reported in our study (Figs. 8, 10, and 12), we hypothesize that the asphaltenes and resins that are the heavy oil components of crude oils are most critical in affecting the IFT behavior between crude oil and brine-surfactant-SiO₂ nanofluids. Furthermore, we also elucidate the potential synergistic effects of NaCl ions from the brine, the asphaltenes and resins, the presence of surfactant, and the SiO₂ NPs on IFTs of crude oil and high salinity brine systems. The content in asphaltenes and resins of the crude oils were ranked as follows: Prudhoe Bay (medium oil) > Lloydminster (heavy oil) > West Texas Intermediate (light oil). Therefore, our study demonstrates that the IFT between the oil-aqueous phase of crude oils containing the highest amount of asphaltenes and resins, which are Prudhoe Bay (medium oil) and Lloydminster (heavy oil) were the two most affected by the brine-surfactant-SiO₂ nanofluid. The IFT between the oil-aqueous phase of the crude oil with the lowest amount of asphaltenes and resins, however, which was the West Texas Intermediate (light oil), was not affected at all by this method. It can be concluded that both the asphaltenes and resins within these crude oils are crucial for the control of the IFT in crude oil-surfactant-nanofluid systems. The most important active component in crude oil for the control of IFT, however, as determined by Cao et al. (2016) was the acidic fraction that is contained in the resin component of all three crude oils examined. Therefore, we conclude that the SiO₂ NPs, the surfactant, and the fractions of asphaltene and resin in crude oil cause the synergistic effect in the oil-surfactant nanofluid interface to decrease the IFT. Although similar synergistic phenomena have been previously reported (Zhang et al. 2014; Lashkarbolooki and Ayatollahi 2016; Lashkarbolooki et al. 2016a, b), further investigations are necessary to elucidate the synergistic mechanisms of these active surfaces at the interfaces between oil-aqueous phases.

Conclusions

The following results were determined from our analysis of the IFT at the oil-aqueous interface for 5 wt% brine-surfactant-SiO₂ nanofluid-oil systems for three oil types, West Texas Intermediate light crude oil, Prudhoe Bay medium crude oil, and Lloydminster heavy crude oil. Specifically, we observed that:

- The SiO₂ nanofluids may either decrease, increase or have no effect whatsoever upon the IFT of brine-surfactant-oil systems.
- The constituents of the oil and aqueous substances do affect the IFT behavior of brine-surfactant-oil systems, with the presence of nanoparticles leading to contrasting IFT trends according to the type of crude oil.
- The IFT increased for the light oil system (0.5 and 2 CMC Tween[®]20) as a function of SiO₂ NPs concentration.
- In terms of the IFT trends, a threshold concentration of SiO₂ NPs occurred for the medium (0.5 and 2 CMC Tween[®]20) and heavy (2 CMC Tween[®]20) oil systems with concentrations above and below this SiO₂ NPs threshold concentration increasing and decreasing the IFT respectively.
- The synergistic/antagonistic effects between crude oil and SiO₂ nanofluids occurred in terms of reducing IFT which decreased until the NP concentrations reached a threshold at which point the synergetic effects between nonionic surfactant and SiO₂ NPs were the opposite and resulted in antagonistic effects.
- The adsorption of both SiO₂ NPs and surfactants at an interface caused a synergistic effect to increase the IFT reduction.
- The asphaltenes and resins are critical components of crude oils for controlling IFT of crude oil-surfactant-nanofluid systems.
- The level of effectiveness of the brine-surfactant-SiO₂ nanofluids in decreasing the IFT between the oil-aqueous phase and mimicking the content of asphaltenes and resins in the crude oils for the three tested crude oils were: (1) Prudhoe Bay > (2) Lloydminster > (3) West Texas Intermediate.
- SiO₂ nanofluids can decrease IFT and therefore capillary pressure to induce the movement and recovery of oil in original water-wet reservoirs.
- SiO₂ nanofluids can increase IFT and, therefore, capillary pressure to increase oil recovery in reservoirs subject to wettability reversal to water-wet conditions.
- Raspberry-like morphology particles were observed in 5 wt% brine-surfactant-SiO₂ nanofluid-oil systems.
- The development of raspberry-like particles material with high surface area, high salt stability, and high capability of interfaces alteration and therefore wettability changes offers a wide range of applications in the fields of applied nanoscience, environmental engineering, and petroleum engineering.

Acknowledgements We wish to convey our appreciation to Clemson University for supporting this work and to Dr. Cindy Lee in the Clemson University Department of Environmental Engineering and Earth Sciences for providing some of the crude oil samples used in

these experiments. We also wish to acknowledge the technical assistance of Linlin Mu in the completion of this study. The authors thank Muhammad Mustafa Hussain, Editor-in-Chief of Applied Nanoscience; and the two reviewers for their useful comments.

Open Access This article is distributed under the terms of the Creative Commons Attribution 4.0 International License (<http://creativecommons.org/licenses/by/4.0/>), which permits unrestricted use, distribution, and reproduction in any medium, provided you give appropriate credit to the original author(s) and the source, provide a link to the Creative Commons license, and indicate if changes were made.

References

- Ahualli S, Iglesias GR, Wachter W et al (2011) Adsorption of anionic and cationic surfactants on anionic colloids: supercharging and destabilization. *Langmuir* 27:9182–9192. <https://doi.org/10.1021/la201242d>
- Amaya J, Rana D, Hornof V (2002) Dynamic interfacial tension behavior of water/oil systems containing in situ-formed surfactants. *J Solut Chem* 31:139–148. <https://doi.org/10.1023/a:1015201119955>
- Bear J (1988) Dynamics of fluids in porous media. Dover Publications Inc., New York
- Binks BP (2002) Particles as surfactants—similarities and differences. *Curr Opin Colloid Interface Sci* 7:21–41. [https://doi.org/10.1016/s1359-0294\(02\)00008-0](https://doi.org/10.1016/s1359-0294(02)00008-0)
- Binks BP, Whitby CP (2005) Nanoparticle silica-stabilised oil-in-water emulsions: improving emulsion stability. *Colloids Surfaces A* 253:105–115. <https://doi.org/10.1016/j.colsurfa.2004.10.116>
- Biswal NR, Singh JK (2016) Interfacial behavior of nonionic Tween 20 surfactant at oil-water interfaces in the presence of different types of nanoparticles. *Rsc Adv* 6:113307–113314. <https://doi.org/10.1039/c6ra23093h>
- Biswal NR, Rangera N, Singh JK (2016) Effect of different surfactants on the interfacial behavior of the n-hexane-water system in the presence of silica nanoparticles. *J Phys Chem B* 120:7265–7274. <https://doi.org/10.1021/acs.jpcc.6b03763>
- Bouchard D, Zhang W, Powell T, Rattanaudompol US (2012) Aggregation kinetics and transport of single-walled carbon nanotubes at low surfactant concentrations. *Environ Sci Technol* 46:4458–4465. <https://doi.org/10.1021/es204618v>
- Brian BW, Chen JC (1987) Surface-tension of solid-liquid slurries. *AIChE J* 33:316–318. <https://doi.org/10.1002/aic.690330220>
- Cao JH, Zhou ZH, Xu ZC et al (2016) Synergism/antagonism between crude oil fractions and novel betaine solutions in reducing interfacial tension. *Energy Fuels* 30:924–932. <https://doi.org/10.1021/acs.energyfuels.5b02566>
- Carcouet CCM (2014) Chemistry and morphology of silica nanoparticles. Eindhoven: Technische Universiteit Eindhoven. <https://doi.org/10.6100/IR762547>. <http://repository.tue.nl/762547>. Accessed 26 Oct 2017
- Carcouet C, van de Put MWP, Mezari B et al (2014) Nucleation and growth of monodisperse silica nanoparticles. *Nano Lett* 14:1433–1438. <https://doi.org/10.1021/nl404550d>
- Chen Q, Saltiel C, Manickavasagam S et al (2004) Aggregation behavior of single-walled carbon nanotubes in dilute aqueous suspension. *J Colloid Interface Sci* 280:91–97. <https://doi.org/10.1016/j.jcis.2004.07.028>
- Cieslinski JT, Krygier KA (2014) Sessile droplet contact angle of water-Al₂O₃, water-TiO₂ and water-Cu nanofluids. *Exp Therm Fluid Sci* 59:258–263. <https://doi.org/10.1016/j.expthermflusci.2014.06.004>
- Defay R, Prigoin I (1966) Surface tension and adsorption. Wiley, New York
- Donaldson EC, Chilingarian GV, Yen TF (1989) Enhanced oil recovery, II: processes and operations. Elsevier Science Publishers B.V., Amsterdam
- Dong LC, Johnson D (2003) Surface tension of charge-stabilized colloidal suspensions at the water-air interface. *Langmuir* 19:10205–10209. <https://doi.org/10.1021/la035128j>
- Ehtesabi H, Ahadian MM, Taghikhani V, Ghazanfari MH (2014) Enhanced heavy oil recovery in sandstone cores using TiO₂ nanofluids. *Energy Fuels* 28:423–430. <https://doi.org/10.1021/ef401338c>
- Elder KR, Grant M, Provatas N, Kosterlitz JM (2001) Sharp interface limits of phase-field models. *Phys Rev E*. <https://doi.org/10.1103/PhysRevE.64.021604>
- Environment Canada (2017a) West Texas Intermediate. http://www.etc-cte.ec.gc.ca/databases/OilProperties/pdf/WEST_Texas_Intermediate.pdf. Accessed 16 May 2017
- Environment Canada (2017b) Prudhoe Bay. [http://www.etc-cte.ec.gc.ca/databases/OilProperties/pdf/WEST_Prudhoe_Bay_\(1995\).pdf](http://www.etc-cte.ec.gc.ca/databases/OilProperties/pdf/WEST_Prudhoe_Bay_(1995).pdf). Accessed 16 May 2017
- Environment Canada (2017c) Lloydminster. http://www.etc-cte.ec.gc.ca/databases/OilProperties/pdf/WEST_Lloydminster.pdf. Accessed 16 May 2017
- Eskandar NG, Simovic S, Prestidge CA (2007) Synergistic effect of silica nanoparticles and charged surfactants in the formation and stability of submicron oil-in-water emulsions. *Phys Chem Chem Phys* 9:6426–6434. <https://doi.org/10.1039/b710256a>
- Esmailzadeh P, Hosseinpour N, Bahramian A et al (2014) Effect of ZrO₂ nanoparticles on the interfacial behavior of surfactant solutions at air-water and n-heptane-water interfaces. *Fluid Phase Equilib* 361:289–295. <https://doi.org/10.1016/j.fluid.2013.11.014>
- Espinasse B, Hotze EM, Wiesner MR (2007) Transport and retention of colloidal aggregates of C-60 in porous media: effects of organic macromolecules, ionic composition, and preparation method. *Environ Sci Technol* 41:7396–7402. <https://doi.org/10.1021/es0708767>
- Fan X, Zheng LF, Cheng J et al (2012) Template synthesis of raspberry-like polystyrene/SiO₂ composite microspheres and their application in wettability gradient surfaces. *Surf Coat Technol* 213:90–97. <https://doi.org/10.1016/j.surfcoat.2012.10.025>
- Fang J, Shan XQ, Wen B, Huang RX (2013) Mobility of TX100 suspended multiwalled carbon nanotubes (MWCNTs) and the facilitated transport of phenanthrene in real soil columns. *Geoderma* 207:1–7. <https://doi.org/10.1016/j.geoderma.2013.04.035>
- Fletcher A, Davis J (2010) How EOR can be transformed by nanotechnology. In: Soc. Pet. Eng. Symp. Improv. Oil Recover. SPE-129531-MS
- Fu KF, Sun YP (2003) Dispersion and solubilization of carbon nanotubes. *J Nanosci Nanotechnol* 3:351–364. <https://doi.org/10.1166/jnn.2003.225>
- Ganguly S, Chakraborty S (2011) Sedimentation of nanoparticles in nanoscale colloidal suspensions. *Phys Lett A* 375:2394–2399. <https://doi.org/10.1016/j.physleta.2011.04.018>
- Ghadimi A, Metselaar IH (2013) The influence of surfactant and ultrasonic processing on improvement of stability, thermal conductivity and viscosity of titania nanofluid. *Exp Therm Fluid Sci* 51:1–9. <https://doi.org/10.1016/j.expthermflusci.2013.06.001>
- Ghezzi F, Earnshaw JC, Finnis M, McCluney M (2001) Pattern formation in colloidal monolayers at the air-water interface.

- J Colloid Interface Sci 238:433–446. <https://doi.org/10.1006/jcis.2001.7495>
- Godinez IG, Darnault CJG (2011) Aggregation and transport of nano-TiO₂ in saturated porous media: effects of pH, surfactants and flow velocity. *Water Res* 45:839–851. <https://doi.org/10.1016/j.watres.2010.09.013>
- Godinez IG, Darnault CJG, Khodadoust AP, Bogdan D (2013) Deposition and release kinetics of nano-TiO₂ in saturated porous media: effects of solution ionic strength and surfactants. *Environ Pollut* 174:106–113. <https://doi.org/10.1016/j.envpol.2012.11.002>
- Gonzenbach UT, Studart AR, Tervoort E, Gauckler LJ (2006) Stabilization of foams with inorganic colloidal particles. *Langmuir* 22:10983–10988. <https://doi.org/10.1021/la061825a>
- Griffith N, Ahmad Y, Daigle H, Huh C (2016) Nanoparticle-stabilized natural gas liquid-in-water emulsions for residual oil recovery. In: Soc. Pet. Eng. Symp. Improv. Oil Recover. SPE-179640-MS
- Hendraningrat L, Torsæter O (2014) Effects of the initial rock wettability on silica-based nanofluid-enhanced oil recovery processes at reservoir temperatures. *Energy Fuels* 28:6228–6241. <https://doi.org/10.1021/ef5014049>
- Hendraningrat L, Torsæter O (2015a) A stabilizer that enhances the oil recovery process using silica-based nanofluids. *Transp Porous Media* 108:679–696. <https://doi.org/10.1007/s11242-015-0495-8>
- Hendraningrat L, Torsæter O (2015b) Metal oxide-based nanoparticles: revealing their potential to enhance oil recovery in different wettability systems. *Appl Nanosci* 5:181–199. <https://doi.org/10.1007/s13204-014-0305-6>
- Hendraningrat L, Li SD, Torsæter O (2013) A coreflood investigation of nanofluid enhanced oil recovery. *J Pet Sci Eng* 111:128–138. <https://doi.org/10.1016/j.petrol.2013.07.003>
- Hu ZL, Azmi SM, Raza G et al (2016a) Nanoparticle-assisted waterflooding in Berea sandstones. *Energy Fuels* 30:2791–2804. <https://doi.org/10.1021/acs.energyfuels.6b00051>
- Hu C, West KR, Scherman OA (2016b) Hollow mesoporous raspberry-like colloids with removable caps as photoresponsive nanocontainers. *Nanoscale* 8:7840–7844. <https://doi.org/10.1039/c6nr01016d>
- Huibers BMJ, Pales AR, Bai L et al (2017) Wettability alteration of sandstones by silica nanoparticle dispersions in light and heavy crude oil. *J Nanopart Res* 19:323. <https://doi.org/10.1007/s11051-017-4011-7>
- Hyung H, Fortner JD, Hughes JB, Kim JH (2007) Natural organic matter stabilizes carbon nanotubes in the aqueous phase. *Environ Sci Technol* 41:179–184. <https://doi.org/10.1021/es061817g>
- Jadhunandan PP, Morrow NR (1995) Effect of wettability on waterflood recovery for crude-oil brine rock systems. *Spe Reserv Eng* 10:40–46. <https://doi.org/10.2118/22597-pa>
- Jaisi DP, Saleh NB, Blake RE, Elimelech M (2008) Transport of single-walled carbon nanotubes in porous media: filtration mechanisms and reversibility. *Environ Sci Technol* 42:8317–8323. <https://doi.org/10.1021/es801641v>
- Jiang LQ, Gao L, Sun J (2003) Production of aqueous colloidal dispersions of carbon nanotubes. *J Colloid Interface Sci* 260:89–94. [https://doi.org/10.1016/s0021-9797\(02\)00176-5](https://doi.org/10.1016/s0021-9797(02)00176-5)
- Joonaki E, Ghanaatian S (2014) The application of nanofluids for enhanced oil recovery: effects on interfacial tension and coreflooding Process. *Pet Sci Technol* 32:2599–2607. <https://doi.org/10.1080/10916466.2013.855228>
- Karimi A, Fakhroueian Z, Bahramian A et al (2012) Wettability alteration in carbonates using zirconium oxide nanofluids: EOR implications. *Energy Fuels* 26:1028–1036. <https://doi.org/10.1021/ef201475u>
- Kasel D, Bradford SA, Simunek J et al (2013) Transport and retention of multi-walled carbon nanotubes in saturated porous media: effects of input concentration and grain size. *Water Res* 47:933–944. <https://doi.org/10.1016/j.watres.2012.11.019>
- Kresge CT, Leonowicz ME, Roth WJ et al (1992) Ordered mesoporous molecular-sieves synthesized by a liquid-crystal template mechanism. *Nature* 359:710–712. <https://doi.org/10.1038/359710a0>
- Lan Q, Yang F, Zhang SY et al (2007) Synergistic effect of silica nanoparticle and cetyltrimethyl ammonium bromide on the stabilization of O/W emulsions. *Colloids Surfaces A* 302:126–135. <https://doi.org/10.1016/j.colsurfa.2007.02.010>
- Lanphere JD, Rogers B, Luth C et al (2014) Stability and transport of graphene oxide nanoparticles in groundwater and surface water. *Environ Eng Sci* 31:350–359. <https://doi.org/10.1089/ees.2013.0392>
- Lashkarbolooki M, Ayatollahi S (2016) Effect of asphaltene and resin on interfacial tension of acidic crude oil/sulfate aqueous solution: experimental study. *Fluid Phase Equilib* 414:149–155. <https://doi.org/10.1016/j.fluid.2016.01.032>
- Lashkarbolooki M, Riazi M, Ayatollahi S (2016a) Investigation of effects of salinity, temperature, pressure, and crude oil type on the dynamic interfacial tensions. *Chem Eng Res Des* 115:53–65. <https://doi.org/10.1016/j.cherd.2016.09.020>
- Lashkarbolooki M, Riazi M, Ayatollahi S, Hezave AZ (2016b) Synergy effects of ions, resin, and asphaltene on interfacial tension of acidic crude oil and low-high salinity brines. *Fuel* 165:75–85. <https://doi.org/10.1016/j.fuel.2015.10.030>
- Lecoanet HF, Wiesner MR (2004) Velocity effects on fullerene and oxide nanoparticle deposition in porous media. *Environ Sci Technol* 38:4377–4382. <https://doi.org/10.1021/es035354f>
- Lecoanet HF, Bottero JY, Wiesner MR (2004) Laboratory assessment of the mobility of nanomaterials in porous media. *Environ Sci Technol* 38:5164–5169. <https://doi.org/10.1021/es0352303>
- Lin DH, Li TT, Yang K, Wu FC (2012) The relationship between humic acid (HA) adsorption on and stabilizing multiwalled carbon nanotubes (MWNTs) in water: effects of HA, MWNT and solution properties. *J Hazard Mater* 241:404–410. <https://doi.org/10.1016/j.jhazmat.2012.09.060>
- Liu XY, O'Carroll DM, Petersen EJ et al (2009) Mobility of multiwalled carbon nanotubes in porous media. *Environ Sci Technol* 43:8153–8158. <https://doi.org/10.1021/es901340d>
- Ma H, Luo M, Dai LL (2008) Influences of surfactant and nanoparticle assembly on effective interfacial tensions. *Phys Chem Chem Phys* 10:2207. <https://doi.org/10.1039/b718427c>
- Matarredona O, Rhoads H, Li ZR et al (2003) Dispersion of single-walled carbon nanotubes in aqueous solutions of the anionic surfactant NaDDBS. *J Phys Chem B* 107:13357–13367. <https://doi.org/10.1021/jp0365099>
- Mattison NT, O'Carroll DM, Rowe RK, Petersen EJ (2011) Impact of porous media grain size on the transport of multi-walled carbon nanotubes. *Environ Sci Technol* 45:9765–9775. <https://doi.org/10.1021/es2017076>
- Meeusen R (2017) The synthesis of raspberry-like particles utilizing a heterocoagulation technique. Hogeschool Utrecht University of Applied Sciences Utrecht. https://www.hbo-kennisbank.nl/en/record/sharekit_hu/oai:surfsharekit.nl:a9a855b6-b1ad-4234-8337-4364bd6a105f. Accessed 26 Oct 2017
- Mekonen A, Sharma P, Fagerlund F (2014) Transport and mobilization of multiwall carbon nanotubes in quartz sand under varying saturation. *Environ Earth Sci* 71:3751–3760. <https://doi.org/10.1007/s12665-013-2769-1>
- Moghadam TF, Azizian S (2014a) Effect of ZnO nanoparticle and hexadecyltrimethylammonium bromide on the dynamic and equilibrium oil–water interfacial tension. *J Phys Chem B* 118:1527–1534. <https://doi.org/10.1021/jp4106986>
- Moghadam TF, Azizian S (2014b) Synergistic effect of ZnO nanoparticles and triblock copolymer surfactant on the dynamic and equilibrium oil–water interfacial tension. *Soft Matter* 10:6192–6197. <https://doi.org/10.1039/c4sm01027b>

- Moghadam TF, Azizian S (2014c) Effect of ZnO nanoparticles on the interfacial behavior of anionic surfactant at liquid/liquid interfaces. *Colloids Surfaces A* 457:333–339. <https://doi.org/10.1016/j.colsurfa.2014.06.009>
- Moghadam TF, Azizian S, Wettig S (2015) Synergistic behaviour of ZnO nanoparticles and gemini surfactants on the dynamic and equilibrium oil/water interfacial tension. *Phys Chem Chem Phys* 17:7122–7129. <https://doi.org/10.1039/c5cp00510h>
- Mohan K, Gupta R, Mohanty KK (2011) Wettability altering secondary oil recovery in carbonate rocks. *Energy Fuels* 25:3966–3973. <https://doi.org/10.1021/ef200449y>
- O'Carroll DM, Liu X, Mattison NT, Petersen EJ (2013) Impact of diameter on carbon nanotube transport in sand. *J Colloid Interface Sci* 390:96–104. <https://doi.org/10.1016/j.jcis.2012.09.034>
- Pales AR, Kinsey EN, Li C et al (2017) Rheological properties of silica nanoparticles in brine and brine-surfactant systems. *J Nanofluids* 6:795–803
- Park S, Lee ES, Sulaiman WRW (2015) Adsorption behaviors of surfactants for chemical flooding in enhanced oil recovery. *J Ind Eng Chem* 21:1239–1245. <https://doi.org/10.1016/j.jiec.2014.05.040>
- Paunov VN, Binks BP, Ashby NP (2002) Adsorption of charged colloid particles to charged liquid surfaces. *Langmuir* 18:6946–6955. <https://doi.org/10.1021/la0203584>
- Pichot R, Spyropoulos F, Norton IT (2012) Competitive adsorption of surfactants and hydrophilic silica particles at the oil-water interface: interfacial tension and contact angle studies. *J Colloid Interface Sci* 377:396–405. <https://doi.org/10.1016/j.jcis.2012.01.065>
- Pu WF, Zhao S, Lu XB et al (2016) The effect of oil properties on oil recovery in dilute surfactant flooding. *Pet Sci Technol* 34:759–764. <https://doi.org/10.1080/10916466.2016.1163398>
- Ranatunga R, Nguyen CT, Wilson BA et al (2011) Molecular dynamics study of nanoparticles and non-ionic surfactant at an oil-water interface. *Soft Matter* 7:6942–6952. <https://doi.org/10.1039/c1sm05145h>
- Ravari RR, Strand S, Austad T (2011) Combined surfactant-enhanced gravity drainage (SEGD) of oil and the wettability alteration in carbonates: the effect of rock permeability and interfacial tension (IFT). *Energy Fuels* 25:2083–2088. <https://doi.org/10.1021/ef200085t>
- Ravera F, Santini E, Loglio G et al (2006) Effect of nanoparticles on the interfacial properties of liquid/liquid and liquid/air surface layers. *J Phys Chem B* 110:19543–19551. <https://doi.org/10.1021/jp0636468>
- Ravera F, Ferrari M, Liggieri L et al (2008) Liquid–liquid interfacial properties of mixed nanoparticle-surfactant systems. *Colloids Surfaces A* 323:99–108. <https://doi.org/10.1016/j.colsurfa.2007.10.017>
- Roosz N, Euvard M, Lakard B et al (2017) Synthesis and characterization of polyaniline-silica composites: raspberry vs core-shell structures. Where do we stand? *J Colloid Interface Sci* 502:184–192. <https://doi.org/10.1016/j.jcis.2017.04.092>
- Roustaei A, Bagherzadeh H (2013) An evaluation of modified silica nanoparticles' efficiency in enhancing oil recovery of light and intermediate oil reservoirs. *Egypt J Pet* 22:427–433
- Roustaei A, Bagherzadeh H (2015) Experimental investigation of SiO₂ nanoparticles on enhanced oil recovery of carbonate reservoirs. *J Pet Explor Prod Technol* 5:27–33. <https://doi.org/10.1007/s13202-014-0120-3>
- Samanta A, Ojha K, Mandal A (2011) The Characterization of natural surfactant and polymer and their Use in enhanced recovery of oil. *Pet Sci Technol* 29:765–777. <https://doi.org/10.1080/10916460903485819>
- Schwartz H, Harel Y, Efrima S (2001) Surface behavior and buckling of silver interfacial colloid films. *Langmuir* 17:3884–3892. <https://doi.org/10.1021/la0100690>
- Sharma T, Iglauer S, Sangwai JS (2016) Silica nanofluids in an oilfield polymer polyacrylamide: interfacial properties, wettability alteration, and applications for chemical enhanced oil recovery. *Ind Eng Chem Res* 55:12387–12397. <https://doi.org/10.1021/acs.iecr.6b03299>
- Somasundaran P, Zhang L (2006) Adsorption of surfactants on minerals for wettability control in improved oil recovery processes. *J Pet Sci Eng* 52:198–212. <https://doi.org/10.1016/j.petrol.2006.03.022>
- Standnes DC, Austad T (2000a) Wettability alteration in chalk 1. Preparation of core material and oil properties. *J Pet Sci Eng* 28:111–121. [https://doi.org/10.1016/s0920-4105\(00\)00083-8](https://doi.org/10.1016/s0920-4105(00)00083-8)
- Standnes DC, Austad T (2000b) Wettability alteration in chalk 2. Mechanism for wettability alteration from oil-wet to water-wet using surfactants. *J Pet Sci Eng* 28:123–143. [https://doi.org/10.1016/s0920-4105\(00\)00084-x](https://doi.org/10.1016/s0920-4105(00)00084-x)
- Stauch C, Spath S, Ballweg T et al (2017) Nanostructured micro-raspberries from superparamagnetic iron oxide nanoparticles: studying agglomeration degree and redispersibility of nanoparticulate powders via magnetisation measurements. *J Colloid Interface Sci* 505:605–614. <https://doi.org/10.1016/j.jcis.2017.06.047>
- Strand S, Standnes DC, Austad T (2003) Spontaneous imbibition of aqueous surfactant solutions into neutral to oil-wet carbonate cores: effects of brine salinity and composition. *Energy Fuels* 17:1133–1144. <https://doi.org/10.1021/ef030051s>
- Strand S, Austad T, Puntervold T et al (2008) “Smart water” for oil recovery from fractured limestone: a preliminary study. *Energy Fuels* 22:3126–3133. <https://doi.org/10.1021/ef800062n>
- Suleimanov BA, Ismailov FS, Veliyev EF (2011) Nanofluid for enhanced oil recovery. *J Pet Sci Eng* 78:431–437. <https://doi.org/10.1016/j.petrol.2011.06.014>
- Tabrizy VA, Hamouda AA, Denoyel R (2011) Influence of magnesium and sulfate ions on wettability alteration of calcite, quartz, and kaolinite: surface energy analysis. *Energy Fuels* 25:1667–1680. <https://doi.org/10.1021/ef200039m>
- Uyusur B, Darnault CJG, Snee PT et al (2010) Coupled effects of solution chemistry and hydrodynamics on the mobility and transport of quantum dot nanomaterials in the vadose zone. *J Contam Hydrol* 118:184–198. <https://doi.org/10.1016/j.jconhyd.2010.09.013>
- Uzelac B, Valmacco V, Trefalt G (2017) Interactions between silica particles in the presence of multivalent cations. *Soft Matter* 13:5741–5748. <https://doi.org/10.1039/c7sm01168g>
- Wang H, Zhou W, Ho DL et al (2004) Dispersing single-walled carbon nanotubes with surfactants: a small angle neutron scattering study. *Nano Lett* 4:1789–1793. <https://doi.org/10.1021/nl048969z>
- Wang YG, Li YS, Fortner JD et al (2008a) Transport and retention of nanoscale C-60 aggregates in water-saturated porous media. *Environ Sci Technol* 42:3588–3594. <https://doi.org/10.1021/es800128m>
- Wang YG, Li YS, Pennell KD (2008b) Influence of electrolyte species and concentration on the aggregation and transport of fullerene nanoparticles in quartz sands. *Environ Toxicol Chem* 27:1860–1867. <https://doi.org/10.1897/08-039.1>
- Wang YF, Xu HM, Yu WZ et al (2011) Surfactant induced reservoir wettability alteration: recent theoretical and experimental advances in enhanced oil recovery. *Pet Sci* 8:463–476. <https://doi.org/10.1007/s12182-011-0164-7>
- Wu YF, Shuler PJ, Blanco M et al (2008) An experimental study of wetting behavior and surfactant EOR in carbonates with model compounds. *Spe J* 13:26–34

- Yu L, Evje S, Kleppe H, et al (2008) Analysis of the wettability alteration process during seawater imbibition into preferentially oil-wet chalk cores. In: Soc. Pet. Eng. Symp. Improv. Oil Recover. SPE-113304-MS
- Yu H, Yoon KY, Neilson BM et al (2014) Transport and retention of aqueous dispersions of superparamagnetic nanoparticles in sandstone. *J Pet Sci Eng* 116:115–123. <https://doi.org/10.1016/j.petrol.2013.08.053>
- Yu MG, Wang Q, Zhang M et al (2017) Facile fabrication of raspberry-like composite microspheres for the construction of superhydrophobic films and applications in highly efficient oil–water separation. *Rsc Adv* 7:39471–39479. <https://doi.org/10.1039/c7ra07250c>
- Yuan CD, Pu WF, Wang XC et al (2015) Effects of interfacial tension, emulsification, and surfactant concentration on oil recovery in surfactant flooding process for high temperature and high salinity reservoirs. *Energy Fuels* 29:6165–6176. <https://doi.org/10.1021/acs.energyfuels.5b01393>
- Zanini M, Hsu CP, Magrini T et al (2017) Fabrication of rough colloids by heteroaggregation. *Colloids Surfaces A* 532:116–124. <https://doi.org/10.1016/j.colsurfa.2017.05.084>
- Zargartalebi M, Barati N, Kharrat R (2014) Influences of hydrophilic and hydrophobic silica nanoparticles on anionic surfactant properties: interfacial and adsorption behaviors. *J Pet Sci Eng* 119:36–43. <https://doi.org/10.1016/j.petrol.2014.04.010>
- Zargartalebi M, Kharrat R, Barati N (2015) Enhancement of surfactant flooding performance by the use of silica nanoparticles. *Fuel* 143:21–27. <https://doi.org/10.1016/j.fuel.2014.11.040>
- Zhang H, Nikolov A, Wasan D (2014) Enhanced oil recovery (EOR) using nanoparticle dispersions: underlying mechanism and imbibition experiments. *Energy Fuels* 28:3002–3009. <https://doi.org/10.1021/ef500272r>
- Zhao CX, Middelberg APJ (2013) Microfluidic synthesis of monodisperse hierarchical silica particles with raspberry-like morphology. *Rsc Adv* 3:21227–21230. <https://doi.org/10.1039/c3ra42362j>

Publisher's Note

Springer Nature remains neutral with regard to jurisdictional claims in published maps and institutional affiliations.